Rabi and Ramsey oscillations of a Majorana qubit in a quantum dot-superconductor array

Pan, Haining; Das Sarma, Sankar; Liu, Chun Xiao

DOI
10.1103/PhysRevB.111.075416

Publication date
2025

Document Version
Final published version

Published in
Physical Review B

Editors' Suggestion

Rabi and Ramsey oscillations of a Majorana qubit in a quantum dot-superconductor array

Haining Pan [1], Sankar Das Sarma,[2] and Chun-Xiao Liu [3,*]

[1]*Department of Physics and Astronomy, Center for Materials Theory, Rutgers University, Piscataway, New Jersey 08854, USA*

[2]*Condensed Matter Theory Center and Joint Quantum Institute, Department of Physics, University of Maryland, College Park, Maryland 20742, USA*

[3]*QuTech and Kavli Institute of NanoScience, Delft University of Technology, Delft, The Netherlands*

(Received 31 July 2024; revised 20 January 2025; accepted 27 January 2025; published 12 February 2025)

The Kitaev chain can be engineered within a quantum dot-superconductor array, hosting Majorana zero modes at fine-tuned sweet spots. In this work, we propose and simulate the occurrence of Rabi and Ramsey oscillations to feasibly construct a minimal Majorana qubit in the quantum dot setup. Our real-time results incorporate realistic effects, e.g., charge noise and leakage, reflecting the latest experimental progress. We demonstrate that Majorana qubits with larger energy gaps exhibit significantly enhanced performance—longer dephasing times, higher quality factors, reduced leakage probabilities, and improved visibilities—compared to those with smaller gaps and with conventional quantum-dot-based charge qubits. We introduce a method for reading out Majorana qubits via quantum capacitance measurements. Our work paves the way for future experiments on realizing Majorana qubits in quantum dot-superconductor arrays.

DOI: 10.1103/PhysRevB.111.075416

I. INTRODUCTION

Majorana zero modes are non-Abelian anyonic excitations localized at the defects or edges of a topological superconductor [1–16]. Qubits constructed from the Majorana excitations are immune to local noise and are fault tolerant without active error corrections, offering a pathway to implementing error-resilient topological quantum computing [3,9]. Recently, the quantum dot-superconductor array has become a promising candidate for realizing topological Kitaev chains [2] in solid-state physics using a concrete idea proposed a while ago [17]. An advantage of this quantum-dot-based approach is the intrinsic robustness against the effect of disorder that is ubiquitous in semiconductor-superconductor Majorana platforms [18–22]. In addition, utilizing Andreev bound states in a hybrid region as the coupler enables precise control over the relative amplitudes of normal and superconducting interactions between quantum dots [23–27], thus allowing for fine tuning of a quantum dot-superconductor array into a sweet spot with optimally protected Majorana zero modes [2,17,28]. Tunnel spectroscopic signatures of Majoranas have been observed in recent experiments on quantum dots using both nanowires [29–31] and two-dimensional electrons [32].

To decisively establish a Majorana qubit and demonstrate its topologically enhanced coherence, Rabi oscillation experiments on quantum-dot-based Kitaev chains are necessary [33]. Additionally, understanding the topological coherence and obtaining a sufficiently long coherence time is crucial for detecting the non-Abelian statistics of Majorana anyons in fusion [34] or braiding [35,36] experiments. Most importantly (and as we demonstrate in the current work), such a Rabi oscillation experiment is already feasible in currently available platforms [29–32], provided that two such minimal Kitaev chains are interconnected via a common superconducting lead and are normal tunnel coupled at their ends [see Fig. 1(a)].

In the current work, we propose Rabi and Ramsey oscillation experiments in a minimal Majorana qubit composed of double two-site Kitaev chains [see Fig. 1(a)]. Our real-time simulations incorporate realistic effects such as charge noise and leakage to the noncomputational bases. We find that Majorana qubits constructed from large-gap Kitaev chains significantly outperform those with smaller gaps and conventional quantum-dot-based charge qubits in terms of dephasing time, quality factor, leakage probability, and visibility. In addition, we propose a Majorana qubit readout method based on quantum capacitance. Our work demonstrates the optimal route to the first step of establishing a Majorana qubit as a viable experimental entity, which has not been achieved in the 15 years of experiments [37–40] and 25 years of theory [1–3,41–43] on topological quantum computing.

II. SETUP AND HAMILTONIAN

A minimal Majorana qubit consists of double two-site Kitaev chains, as shown in Fig. 1(a). The Hamiltonian is

$$\begin{aligned}\mathcal{H}_{\rm tot} &= \mathcal{H}_L + \mathcal{H}_R + \mathcal{H}_{\rm tunn},\\ \mathcal{H}_a &= \sum_{i=1}^{2} \mu_{ai} n_{ai} + (t_a c_{a2}^\dagger c_{a1} + \Delta_a c_{a2} c_{a1} + \text{H.c.}),\\ \mathcal{H}_{\rm tunn} &= \Gamma c_{R1}^\dagger c_{L2} + \text{H.c.}\end{aligned} \tag{1}$$

Here, $\mathcal{H}_a$ with $a \in \{L, R\}$ is the Hamiltonian for the left and right chain, respectively, with μ_{ai} $(i = 1, 2)$ the on-site

*Contact author: chunxiaoliu62@gmail.com

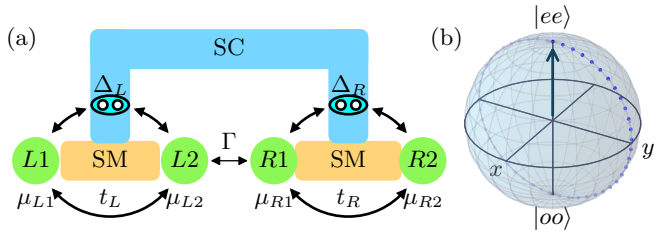

FIG. 1. (a) Schematic of a Majorana qubit composed of double two-site Kitaev chains. (b) Bloch sphere. $|\pm z\rangle$ are defined as $|ee\rangle$ and $|oo\rangle$, respectively. The dots represent the trajectory of the state vector in a Rabi experiment.

energy of a spin-polarized dot orbital, $n_{ai} = c_{ai}^\dagger c_{ai} = 0, 1$ the occupancy number, and t_a and Δ_a the strengths of the normal and Andreev tunnelings. $H_{\rm tunn}$ is the tunnel Hamiltonian, with Γ being the strength of single-electron transfer between dots from different chains. In the current work, we are particularly interested in the sweet spot of the system, which is defined as $\mu_{ai} = 0$ and $t_a = \Delta_a$. Although Δ_L and Δ_R can be different in strength, in the current work we assume them to be equal to simplify the discussions. At that point, the even-parity ground state $|e\rangle_a = (|00\rangle_a - |11\rangle_a)/\sqrt{2}$ is degenerate with the odd-parity one $|o\rangle_a = (|10\rangle_a - |01\rangle_a)/\sqrt{2}$ within each Kitaev chain, hosting a pair of Majorana zero modes at two separate quantum dots. Here, $|n_1 n_2\rangle_a = (c_{a1}^\dagger)^{n_1}(c_{a2}^\dagger)^{n_2}|0\rangle_a$, and $|0\rangle_a$ is the vacuum state of chain a. Since total fermion parity is conserved in the Hamiltonian of Eq. (1), we can focus on the subspace with total parity even without loss of generality. As such, the ground-state degeneracy is twofold,

$$|ee\rangle \equiv |e\rangle_L \otimes |e\rangle_R, \quad |oo\rangle \equiv |o\rangle_L \otimes |o\rangle_R, \tag{2}$$

which form the basis states of a Majorana qubit.

Rabi oscillations. In the qubit subspace spanned by $|ee\rangle$ and $|oo\rangle$, the low-energy effective Hamiltonian is

$$H_{\rm eff} = \frac{\varepsilon}{2}\sigma_z + \frac{\Gamma}{2}\sigma_x, \tag{3}$$

where $\varepsilon \equiv E_{oo} - E_{ee}$ and $\sigma_{x/z}$ are Pauli X/Z matrices. Here, σ_z rotation is proportional to the ground-state energy splitting, which we choose to be $\varepsilon = t_L - \Delta_L$ by detuning the hybrid region in the left chain away from the sweet spot [30]. σ_x rotation is realized by single-electron tunneling between the two chains that can be controlled by a tunnel barrier. Motivated by the form of $H_{\rm eff}$ in Eq. (3), we perform a numerical simulation of the Rabi and Ramsey experiments using the total Hamiltonian $\mathcal{H}_{\rm tot}$ in Eq. (1). Here we implement the qubit rotations by applying sequences of pulses of ε or Γ instead of microwave driving because of the basis state degeneracy. In particular, in the Rabi experiment, the system is initialized in $|ee\rangle$ of two decoupled Kitaev chains at their sweet spots. This corresponds to the north pole of the Bloch sphere. We then turn on the interchain tunneling Γ and let the system evolve for a time τ before performing a readout in the σ_z basis [see pulse profiles in Fig. 2(a)]. Figure 2(b) shows the numerically calculated $P_{ee}(\tau) \equiv |\langle ee|\psi(\tau)\rangle|^2$ in the (Γ, τ) plane. Indeed, the fringe pattern of Rabi oscillations confirms that single-electron tunneling $H_{\rm tunn}$ in Eq. (1) works as a σ_x rotation in the qubit subspace, with the oscillation frequency being

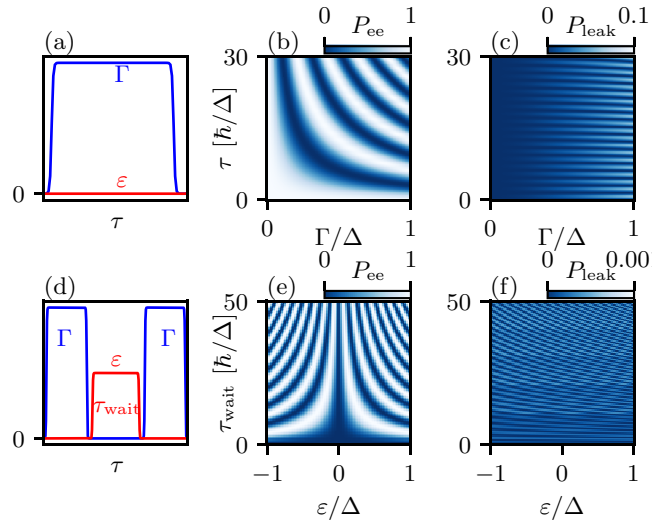

FIG. 2. Numerical simulations in the clean limit. Upper panels: Numerical simulation of a Rabi experiment. (a) Pulse profiles. (b), (c) P_{ee} and $P_{\rm leak}$ in Eq. (7) in the (Γ, τ) plane. Lower panels: Numerical simulation of a Ramsey experiment. (d) Pulse profiles. (e), (f) P_{ee} and $P_{\rm leak}$ in the $(\varepsilon, \tau_{\rm wait})$ plane. Here, $\Delta_L = \Delta_R = \Delta$.

proportional to Γ. However, surprisingly, we also find that the state wave function can leak out of the qubit subspace with a probability $P_{\rm leak}(\tau) \equiv 1 - P_{ee}(\tau) - P_{oo}(\tau)$, which oscillates periodically in time and increases with the tunneling strength Γ [see Fig. 2(c)]. Using time-dependent perturbation theory (see Appendix B), we show that a finite interchain tunneling Γ inevitably induces a leakage to the excited states of $|e'e'\rangle$ and $|o'o'\rangle$, i.e.,

$$P_{\rm leak}(\tau) = P_{e'e'}(\tau) + P_{o'o'}(\tau) \approx \frac{\Gamma^2}{16\Delta^2}\sin^2(2\Delta\tau/\hbar), \tag{4}$$

where $|e'\rangle_a = (|00\rangle_a + |11\rangle_a)/\sqrt{2}$ and $|o'\rangle_a = (|10\rangle_a + |01\rangle_a)/\sqrt{2}$ are excited states in each chain and $\Delta_L = \Delta_R = \Delta$. Here the oscillation frequency of the leakage probability is $4\Delta/\hbar$ and the magnitude scales with Γ^2/Δ^2. On the other hand, in a Ramsey experiment, we first apply a pulse of $H_{\rm tunn}$ to rotate the initial state $|ee\rangle$ to the equator of the Bloch sphere, then let it evolve for a time duration $\tau_{\rm wait}$ in the presence of a finite ε, and apply the same $H_{\rm tunn}$ pulse again before the final readout [see pulse profiles in Fig. 2(d)]. The simulated $P_{ee}(\tau)$ in the $(\varepsilon, \tau_{\rm wait})$ plane is shown in Fig. 2(e). Here the small $P_{\rm leak}$ in Fig. 2(f) is due to the σ_x pulses, while detuning the coupling $t_L - \Delta_L$ has a negligible impact on the leakage probability. Both experiments are doable in the currently available devices and provide complementary information about Majorana coherence.

III. QUBIT DEPHASING

Charge noise is one of the primary sources of decoherence in semiconductor-based qubits [44–51]. It can be induced by charge impurities in the environment or fluctuations in the nearby gate voltages. As a $1/f$ noise, the fluctuations are dominated by the low-frequency components, which can be modeled by the quasistatic disorder approximation, since

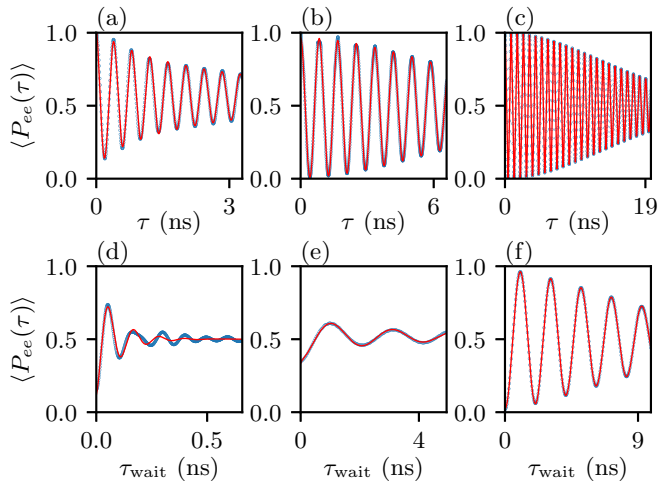

FIG. 3. Numerical simulations including charge noises. Upper panels: Rabi oscillations of disorder-averaged $\langle P_{ee}\rangle$. Lower panels: Ramsey oscillations of disorder-averaged $\langle P_{ee}\rangle$. (a), (d) Semiconductor charge qubits. (b), (e) Small-gap Majorana qubits. (c), (f) Large-gap Majorana qubits. The blue dots are data from numerical simulations, while the red lines are fitting curves using Eq. (5). Here, the size of the disorder ensemble is 500.

the zero-frequency part of the noise dominates [52,53]. That is, in each run of the Rabi or Ramsey experiment, the Hamiltonian parameters in Eq. (1) are subject to a static disorder that obeys normal distribution, and the final readout measurement is averaged over 500 different disorder realizations, giving $\langle P_{ee}(\tau)\rangle$. In particular, we simulate and compare three different types of qubits: (1) a semiconductor charge qubit with one electron in double quantum dots [51,54], (2) a small-gap Majorana qubit [29], and (3) a large-gap Majorana qubit [30,32]. Here a small (large) gap in the Kitaev chain corresponds to the scenario where the dot-hybrid coupling strength is smaller than (comparable to) the induced gap in the hybrid region [55]. The mean values and standard deviations of the Hamiltonian parameters that are subject to charge noises are chosen according to the values reported in relevant experimental works, which are summarized in the Appendix F. Figure 3 shows the calculated Rabi and Ramsey oscillations of $\langle P_{ee}(\tau)\rangle$ with dephasing for all three types of qubits. The curves with decaying envelopes are further fitted using the following formula:

$$\langle P_{ee}(\tau)\rangle = P_0 + A\cos(2\pi f\tau + \phi_0)\exp -(\tau/T_2)^{\beta}, \quad (5)$$

where $2A$ is the visibility, T_2 is the dephasing time, and β is the decaying exponent. Their values are summarized in Table I and, in addition, we define the quality factor as

$$Q = 2\pi f T_2, \quad (6)$$

and the leakage probability as

$$P_{\rm leak} = \lim_{\tau_0\to\infty}\int_0^{\tau_0}\langle P_{\rm leak}(\tau)\rangle d\tau/\tau_0, \quad (7)$$

in the long-time limit where $\langle P_{\rm leak}(\tau)\rangle = 1 - \langle P_{ee}(\tau)\rangle - \langle P_{oo}(\tau)\rangle$ is the instantaneous value.

The Hamiltonian for a semiconductor charge qubit is

$$H_c = \begin{pmatrix}\varepsilon_L & \Gamma\\ \Gamma & \varepsilon_R\end{pmatrix}, \quad (8)$$

where the basis states are $|10\rangle$ and $|01\rangle$ with one electron in the left or right quantum dot, ε_L (ε_R) is the corresponding orbital energy in the left (right) dot, and Γ is the interdot coupling strength. Here, the fluctuations of the dot energies σ_ε dominate the dephasing effect, compared to the fluctuations of the interdot coupling strength σ_Γ, due to the small magnitude of Γ. In the Rabi experiment, the dot energies are tuned into a sweet spot of $\varepsilon_L = \varepsilon_R = 0$, which is insensitive to dot-energy detuning up to the first order, i.e., $\partial E/\partial\varepsilon_a = 0$. However, since the dot-energy fluctuations are large and comparable to the interdot coupling strength, e.g., $\sigma_\varepsilon = 3$ μeV $\simeq$ $\Gamma = 5$ μeV, the higher-order contributions (e.g., $\delta E \sim \sigma_\varepsilon^2/\Gamma$) lead to a short dephasing time $T_2 \approx 2.50(7)$ ns for x rotations; see Fig. 3(a). In the Ramsey experiment, to implement the z rotation, we choose $\varepsilon_L = -\varepsilon_R = 20$ μeV $\gg \Gamma$, which is much more susceptible to charge noise as $\partial E/\partial\varepsilon_a \approx 1$. Thus, the dephasing time is even shorter, $T_2 \approx 0.096(2)$ ns, and the visibility is reduced; see Fig. 3(d). The consistency between our T_2 estimates and the experimental measurements reported in Ref. [54] validates our modeling of the quantum dot devices.

In a minimal two-site Kitaev chain that is in the vicinity of the sweet spot, the energy splitting between the even- and odd-parity ground states is approximately $E \equiv E_o - E_e \approx$

TABLE I. Comparison of qubit performances.

Protocol	Qubit properties	Charge qubit	Small-gap Majorana qubit	Large-gap Majorana qubit
Rabi	T_2 (ns) [Eq. (5)]	2.50(7)	9.25(5)	19.064(8)
	Q [Eq. (6)]	38(1)	69.4(4)	144.7(5)
	$2A$ [Eq. (5)]	1.01(2)	0.958(1)	1.001(3)
	$P_{\rm leak}$ [Eq. (7)]		0.035	$5.7(8)\times10^{-4}$
	β [Eq. (5)]	0.66(2)	1.87(2)	1.941(3)
Ramsey	T_2 (ns) [Eq. (5)]	0.096(2)	1.84(7)	11.23(1)
	Q [Eq. (6)]	5.3(2)	5.6(2)	34.31(3)
	$2A$ [Eq. (5)]	0.77(2)	0.3716(8)	0.950(5)
	$P_{\rm leak}$ [Eq. (7)]		0.0275(1)	$3.31(6)\times10^{-5}$
	β [Eq. (5)]	1.01(4)	0.57(2)	1.557(4)

$\mu_1\mu_2/2t + (t - \Delta)$, where the first term is due to the simultaneous detuning of on-site dot energies, while the second term is the detuning of the hybrid region. In a small-gap Majorana qubit (i.e., small $t \equiv \Delta$ limit), the dot-energy fluctuations are comparatively dominant, giving a characteristic energy splitting between the basis states $\delta E \sim \sigma_\mu^2/t$. For a Majorana qubit defined in Fig. 1(a), such a δE leads to noise in the σ_z basis. In the Rabi experiment, since the dot-energy noise ($\propto \sigma_z$) is orthogonal to the σ_x rotation, the dephasing effect of the dot-energy fluctuations is strongly mitigated (see the Appendix F). As such, $T_2 \approx 9.25(5)$ ns is jointly determined by the fluctuations in the dot energies ($\propto \sigma_z$) as well as in the interchain coupling strengths ($\propto \sigma_x$); see Fig. 3(b). In the Ramsey experiment on σ_z rotations, the large dot-energy fluctuations ($\propto \sigma_z$) cause a more detrimental effect on qubit dephasing, giving a much shorter dephasing time $T_2 \approx 1.84(7)$ ns and a reduced visibility $2A \approx 0.3716(8)$; see Fig. 3(e) and Table I. Note that here the dephasing effect of charge noise in t_a and Δ_a is negligible because of the weak dot-superconductor hybridization.

On the contrary, the performance of a large-gap Majorana qubit is much improved in almost all aspects, e.g., dephasing time, quality factor, visibility, and leakage probability. The strong dot-superconductor hybridization not only strongly enhances the excitation gap of a Kitaev chain, but also transforms the dot orbitals into Yu-Shiba-Rusinov states [56–58], thus significantly screening the electric charge in the quantum dots [30,32,55]. As a result, the energy splitting due to μ_{ai} fluctuations in the effective Kitaev chain is strongly suppressed, i.e., σ_μ^2/t is reduced by a factor of ∼300 compared to the small-gap Majorana qubit. Now the dominant source of dephasing in the Rabi experiment is the charge noise in Γ, giving $T_2 \approx 19.064(8)$ ns; see Fig. 3(c). In the Ramsey experiment, the fluctuations of $t_a - \Delta_a$ begin to dominate the dephasing, giving $T_2 \approx 11.23(1)$ ns; see Fig. 3(f). In addition, a larger excitation gap in the Majorana qubit also greatly suppresses the leakage probabilities (see Table I), consistent with the analytic estimates shown in Eq. (7).

IV. QUBIT READOUT

To read out the Majorana qubits, we consider the quantum capacitance measurement as shown in Fig. 4, which is defined as

$$C_q = -\frac{\partial^2 E}{\partial V_g^2}, \tag{9}$$

in the zero-temperature limit [34]. Here, E is the eigenenergy, and V_g is the gate voltage that controls the dot energy via $\mu_{ai} = \alpha_{ai} V_g$, with α_{ai} being the lever arm. Since the measurement is performed when the two chains are decoupled, the result would simply be a sum of the values in each chain, i.e., $C_q = C_{qL} + C_{qR}$. Furthermore, in the equal-lever-arm regime ($\alpha_{a1} = \alpha_{a2} \equiv \alpha$), the quantum capacitance comes only from the even-parity state within each chain, while that of the odd-parity one is strongly suppressed [34]. Thus the quantum capacitances of $|ee\rangle$ and $|oo\rangle$ are

$$C_q^{ee} = \frac{\alpha^2}{\Delta_L} + \frac{\alpha^2}{\Delta_R}, \quad C_q^{oo} = 0, \tag{10}$$

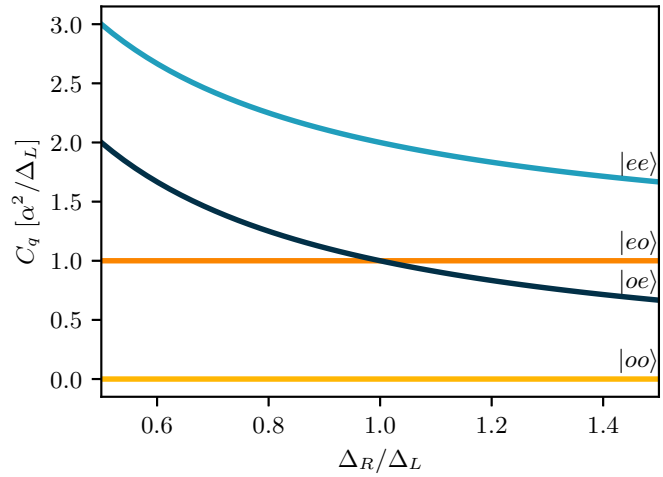

FIG. 4. Quantum capacitance readout in Eq. (9) of the low-energy states in a Majorana qubit. α is the magnitude of the lever arm of the quantum dots, assumed to be identical for all dots. Δ_L (Δ_R) are the superconducting coupling strengths in the left (right) chains.

which are distinct from each other and therefore can be used for qubit readout (see the Appendix G). Following the argument, we further obtain that $C_q^{eo} = \alpha^2/\Delta_L$ and $C_q^{oe} = \alpha^2/\Delta_R$, which are different from both C_q^{ee} and C_q^{oo}. Therefore, in addition to qubit readout, C_q measurement can simultaneously reveal the quasiparticle poisoning effect that transitions a Majorana qubit between states in different total parity space.

V. DISCUSSION

In the numerical simulations, we regard $1/f$ charge noise as the dominant source of decoherence in the proposed devices, neglecting the quasiparticle poisoning effect because this is the prevailing situation in semiconductor platforms. For example, a poisoning time of ∼1 ms, as reported in a similar semiconductor-superconductor hybrid device [59], is much longer than the dephasing time considered here, ∼10 ns, making poisoning insignificant for the current consideration where $1/f$ charge noise dominates decoherence. In addition, here both Rabi and Ramsey experiments are simulated using the most basic protocols for x and z rotations in order to demonstrate the working principles and to provide a fair comparison between semiconductor charge qubits and Majorana qubits. We emphasize that the system we consider [29–32] is equivalent to semiconductor charge qubits if all superconductivity is removed from consideration. It is, therefore, possible to further improve the dephasing time, e.g., by optimizing the pulse profiles, by designing a form of interdot coupling that is more resilient against charge noise, or by further scaling up the Kitaev chain [27,31,60]. Such considerations should be relevant once the basic Rabi and Ramsey oscillations proposed by us are observed so that the elementary concept of a Majorana qubit is established beyond the simplest transport measurements prevalent so far in this subject. We emphasize that our work establishes the feasibility of Rabi oscillations in the already existing experimental platforms of Refs. [29–32].

VI. SUMMARY

We propose and simulate Rabi and Ramsey oscillation experiments for a minimal Majorana qubit defined in coupled quantum dot-superconductor arrays. Our realistic calculations predict actual results of such an experiment and demonstrate that the performance of large-gap Majorana qubits significantly surpasses that of the small-gap counterparts and traditional conventional charge qubits, although some enhancement over semiconductor charge qubits should already manifest in the small-gap platforms. Consequently, conducting such experiments is both feasible and promising on currently available Kitaev chain devices, utilizing existing control and measurement technologies. Our work thus points in an experimental direction of establishing the quantum dot Majorana systems as a viable platform by showing how to perform a completely different experiment, in the context of Majorana systems. This would provide a crucial step toward the realization of the first Majorana qubit in solid-state systems. In fact, the observation of stable Rabi oscillations is synonymous with having a qubit, and our work establishes that such a qubit experiment should be successful in the existing Majorana platforms. The observation of Rabi oscillations in this platform will establish that a feasible qubit exists here, and may also establish that this qubit has substantially enhanced coherence compared with the corresponding semiconductor quantum-dot-based charge qubits with no superconductors.

ACKNOWLEDGMENTS

We are particularly grateful to Xin Zhang, Francesco Zatelli, F. Setiawan, Michael Wimmer, and Jay D. Sau for useful discussions. H.P. is supported by U.S. Office of Naval Research, Grant No. N00014-23-1-2357. C.-X.L. is supported by a subsidy for top consortia for knowledge and innovation (TKI subsidiary). S.D.S. is supported by the Laboratory for Physical Sciences through the Condensed Matter Theory Center at the University of Maryland.

APPENDIX A: MODEL

The system of the double two-site Kitaev chain is described by the following Hamiltonian:

$$\mathcal{H} = \mathcal{H}_L + \mathcal{H}_R + \mathcal{H}_T + \mathcal{H}_\mu, \tag{A1}$$

where intrachain coupling in the left chain (site index 1 and 2) and right chain (site index 3 and 4) is

$$\mathcal{H}_L = t\sum(c_{L2}^\dagger c_{L1} + c_{L1}^\dagger c_{L2}) + \Delta(c_{L2}c_{L1} + c_{L1}^\dagger c_{L2}^\dagger),$$

$$\mathcal{H}_R = t\sum(c_{R2}^\dagger c_{R1} + c_{R1}^\dagger c_{R2}) + \Delta(c_{R2}c_{R1} + c_{R1}^\dagger c_{R2}^\dagger), \tag{A2}$$

the interchain hopping is

$$\mathcal{H}_T = \Gamma(c_{R1}^\dagger c_{L2} + c_{L2}^\dagger c_{R1}), \tag{A3}$$

and the on-site chemical potential is

$$\mathcal{H}_\mu = \sum_{a\in\{L,R\}}\sum_{i=1}^{2}\mu_i c_{a,i}^\dagger c_{a,i}. \tag{A4}$$

Up to a particle-hole transformation, we can choose $t > 0$, $\Delta > 0$, and $\Gamma > 0$.

Here, without the tunneling term $\Gamma = 0$, the two chains are decoupled, where the sweet spot is achieved when $t = \Delta$, and $\mu_i = 0$, leading to the ground-state manifold spanned by

$$|e\rangle_L = \frac{1}{\sqrt{2}}(1 - c_{L1}^\dagger c_{L2}^\dagger)|0\rangle, \quad |o\rangle_L = \frac{1}{\sqrt{2}}(c_{L1}^\dagger - c_{L2}^\dagger)|0\rangle, \tag{A5}$$

$$|e\rangle_R = \frac{1}{\sqrt{2}}(1 - c_{R1}^\dagger c_{R2}^\dagger)|0\rangle, \quad |o\rangle_R = \frac{1}{\sqrt{2}}(c_{R1}^\dagger - c_{R2}^\dagger)|0\rangle, \tag{A6}$$

for the left and right systems, respectively.

With the tunneling term, the ground state of the two chains can be spanned by the two other single-chain excited states denoted as

$$|e'\rangle_L = \frac{1}{\sqrt{2}}(1 + c_{L1}^\dagger c_{L2}^\dagger)|0\rangle, \quad |o'\rangle_L = \frac{1}{\sqrt{2}}(c_{L1}^\dagger + c_{L2}^\dagger)|0\rangle, \tag{A7}$$

$$|e'\rangle_R = \frac{1}{\sqrt{2}}(1 + c_{R1}^\dagger c_{R2}^\dagger)|0\rangle, \quad |o'\rangle_R = \frac{1}{\sqrt{2}}(c_{R1}^\dagger + c_{R2}^\dagger)|0\rangle. \tag{A8}$$

Therefore, $|e\rangle_L$, $|e'\rangle_L$, $|o\rangle_L$, and $|o'\rangle_L$ ($|e\rangle_R$, $|e'\rangle_R$, $|o\rangle_R$, and $|o'\rangle_R$) form the complete basis for the left (right) chain.

Without the loss of generality, we choose to work in the even total parity, leading to a complete basis of $|ee\rangle \equiv |e\rangle_L|e\rangle_R$, $|oo\rangle$, $|e'e'\rangle$, $|o'o'\rangle$, $|ee'\rangle$, $|oo'\rangle$, $|e'e\rangle$, and $|o'o\rangle$. With this set of bases, the matrix representation of the sum of Hamiltonian (A2) and (A3) is

$$H_L + H_R + H_T = \begin{pmatrix} h_+ & 0 \\ 0 & h_- \end{pmatrix}, \tag{A9}$$

where h_+ and h_- are

$$h_+ = \begin{pmatrix} -2\Delta & -\Gamma/2 & 0 & -\Gamma/2 \\ -\Gamma/2 & -2t & \Gamma/2 & 0 \\ 0 & \Gamma/2 & 2\Delta & \Gamma/2 \\ -\Gamma/2 & 0 & \Gamma/2 & 2t \end{pmatrix}, \tag{A10}$$

$$h_- = \begin{pmatrix} 0 & \Gamma/2 & 0 & \Gamma/2 \\ \Gamma/2 & 0 & -\Gamma/2 & 0 \\ 0 & -\Gamma/2 & 0 & -\Gamma/2 \\ \Gamma/2 & 0 & -\Gamma/2 & 0 \end{pmatrix}. \tag{A11}$$

Similarly, the matrix representation of the on-site chemical potential given by Eq. (A4) is

$$H_\mu = \frac{\mu_{1234}}{2}\mathbb{1} + \frac{1}{2}\begin{pmatrix} 0 & h_\mu \\ h_\mu^\dagger & 0 \end{pmatrix}, \tag{A12}$$

where

$$h_\mu = \begin{pmatrix} -\mu_{34} & 0 & -\mu_{12} & 0 \\ 0 & \delta\mu_{34} & 0 & \delta\mu_{12} \\ -\mu_{12} & 0 & -\mu_{34} & 0 \\ 0 & \delta\mu_{12} & 0 & \delta\mu_{34} \end{pmatrix}, \tag{A13}$$

with the shorthand notions of $\mu_{1234} \equiv \sum_{i=1}^{4} \mu_i$, $\mu_{12} \equiv \mu_1 + \mu_2$, $\mu_{34} \equiv \mu_3 + \mu_4$, $\delta\mu_{12} \equiv \mu_1 - \mu_2$, and $\delta\mu_{34} \equiv \mu_3 - \mu_4$.

APPENDIX B: LEAKAGE DUE TO Δ, t, AND Γ

In Eq. (3) in the main text, we considered the disorder effect in ϵ and Γ before σ_z and σ_x. Here, we will consider their leakage effect separately to understand the leakage that is effectively on ϵ and Γ.

We first consider the effect of the disorder only in Δ, t, and Γ, i.e., $\mu_i = 0$, because Eq. (A9) is block diagonal, and given the initial state is $|ee\rangle$, we only need to consider the subspace of h_+, where the Rabi oscillation is between $|ee\rangle$ and $|oo\rangle$ and the leakage states are $|e'e'\rangle$ and $|o'o'\rangle$.

We use the time-dependent perturbation theory, where Eq. (A9) is decomposed into the noninteracting part H_0,

$$H_0 = \begin{pmatrix} -2\Delta & -\Gamma/2 & 0 & 0 \\ -\Gamma/2 & -2t & 0 & 0 \\ 0 & 0 & 2\Delta & \Gamma/2 \\ 0 & 0 & \Gamma/2 & 2t \end{pmatrix}, \tag{B1}$$

and the perturbation H_1 as

$$H_1 = \begin{pmatrix} 0 & 0 & 0 & -\Gamma/2 \\ 0 & 0 & \Gamma/2 & 0 \\ 0 & \Gamma/2 & 0 & 0 \\ -\Gamma/2 & 0 & 0 & 0 \end{pmatrix}. \tag{B2}$$

Conceptually, the first term H_0 in Eq. (B1) accounts for the Rabi oscillation between $|ee\rangle$ and $|oo\rangle$ (given the initial state is $|ee\rangle$), and the second term H_1 in Eq. (B2) leads to $|e'e'\rangle$ and $|o'o'\rangle$.

The time-evolution operator (in the Schrödinger picture) is expanded in the Dyson series (truncated at the first order) as

$$U(\tau) = e^{-iH_0\tau}\left[1 - i\int_0^\tau d\tau_1 H_{1,I}(\tau_1)\right]e^{iH_0\tau}, \tag{B3}$$

where $H_{1,I}(\tau_1)$ is H_1 in the interacting picture,

$$H_{1,I}(\tau_1) = e^{iH_0\tau}H_1 e^{-iH_0\tau} = \sum_{i,j}\langle i|H_1|j\rangle e^{i(E_i-E_j)\tau_1}, \tag{B4}$$

and $|i\rangle$ is the eigenvector of H_0 with the eigenvalues of E_i.

The spectrum of H_0 in Eq. (B1) is

$$\begin{aligned} -E_+ &: \quad \left(\cos\left(\tfrac{\theta}{2}\right) \quad \sin\left(\tfrac{\theta}{2}\right) \quad 0 \quad 0\right)^\intercal, \\ -E_- &: \quad \left(-\sin\left(\tfrac{\theta}{2}\right) \quad \cos\left(\tfrac{\theta}{2}\right) \quad 0 \quad 0\right)^\intercal, \\ E_- &: \quad \left(0 \quad 0 \quad -\sin\left(\tfrac{\theta}{2}\right) \quad \cos\left(\tfrac{\theta}{2}\right)\right)^\intercal, \\ E_+ &: \quad \left(0 \quad 0 \quad \cos\left(\tfrac{\theta}{2}\right) \quad \sin\left(\tfrac{\theta}{2}\right)\right)^\intercal, \end{aligned} \tag{B5}$$

where $E_\pm = \Delta + t \pm \sqrt{(\Delta - t)^2 + (\Gamma/2)^2}$ and $\tan\theta = \frac{\Gamma/2}{\Delta - t}$. We substitute the eigenvectors and eigenvalues of H_0 into Eq. (B4), with the initial state

$$|\psi(\tau = 0)\rangle = |ee\rangle = (1 \quad 0 \quad 0 \quad 0)^\intercal, \tag{B6}$$

and we have the (unnormalized) final state in the Schrödinger picture as

$$\begin{aligned} |\psi(\tau)\rangle &= U(\tau)|\psi(\tau = 0)\rangle = |\psi(\tau)\rangle \\ &= \begin{pmatrix} e^{i\omega\tau}[\cos(\Omega\tau) + i\sin(\Omega\tau)\cos\theta] \\ e^{i\omega\tau} i\sin(\Omega\tau)\sin\theta \\ \frac{\Gamma}{2\omega}\sin(\omega\tau)\sin(\Omega\tau)\sin\theta \\ \frac{\Gamma}{2\omega}[-\sin(\Omega\tau)\cos\theta + i\cos(\Omega\tau)]\sin(\omega\tau) \end{pmatrix}, \end{aligned} \tag{B7}$$

where $\Omega = \sqrt{(\Delta - t)^2 + (\Gamma/2)^2}$ and $\omega = \Delta + t$.

Therefore, the Rabi oscillations between $|ee\rangle$ and $|oo\rangle$ have the probability densities of

$$\begin{aligned} P_{ee}(\tau) &= |\langle ee|\psi(\tau)\rangle|^2 = \sin^2(\Omega\tau)\cos^2(\theta) + \cos^2(\Omega\tau), \\ P_{oo}(\tau) &= |\langle oo|\psi(\tau)\rangle|^2 = \sin^2(\theta)\sin^2(\Omega\tau), \end{aligned} \tag{B8}$$

and the leakage is

$$\begin{aligned} P_{\text{leak}}(\tau) &= P_{e'e'}(\tau) + P_{o'o'}(\tau) = |\langle e'e'|\psi(\tau)\rangle|^2 + |\langle o'o'|\psi(\tau)\rangle|^2 \\ &= \frac{\Gamma^2\sin^2(\omega\tau)}{4\omega^2}, \end{aligned} \tag{B9}$$

indicating that the leakage frequency is $2\omega = 2(\Delta + t)$, which is independent of the Γ and consistent with Fig. 2(b) in the main text.

Specifically, at the sweep spot $\Delta = t$, we have $\theta = \pi/2$ and the probability densities are

$$\begin{aligned} P_{ee}(\tau) &= \cos^2(\Omega\tau), \\ P_{oo}(\tau) &= \sin^2(\Omega\tau), \\ P_{\text{leak}}(\tau) &= \frac{\Gamma^2}{16\Delta^2}\sin^2(2\Delta\tau), \end{aligned} \tag{B10}$$

recovering the Rabi frequency $2\Omega = \Gamma$ in Fig. 2(a).

APPENDIX C: LEAKAGE DUE TO μ_1

To consider the leakage effect in μ_1 (or, equivalently, for μ_4 due to the inversion symmetry), we set all other parameters to the sweet spot, including $\Delta = t_0$ and $\mu_2 = \mu_3 = \mu_4 = 0$. Following the same time-dependent perturbation theory, the noninteracting part $H_0^{\mu_1}$ is

$$H_0^{\mu_1} = \frac{\mu_1}{2}\mathbb{1} + \begin{pmatrix} H_0 & 0 \\ 0 & h_- \end{pmatrix}, \tag{C1}$$

where H_0 and h_- are in Eq. (B1) and in Eq. (A11) (with $\Delta = t$), and the perturbation term $H_1^{\mu_1}$ is

$$H_1^{\mu_1} = \begin{pmatrix} H_1 & h_{\mu_1} \\ h_{\mu_1}^\dagger & 0 \end{pmatrix}, \tag{C2}$$

where H_1 is in Eq. (B2) and H_{μ_1} is

$$h_{\mu_1} = \frac{1}{2}\begin{pmatrix} 0 & 0 & -\mu_1 & 0 \\ 0 & 0 & 0 & \mu_1 \\ -\mu_1 & 0 & 0 & 0 \\ 0 & \mu_1 & 0 & 0 \end{pmatrix}, \tag{C3}$$

from Eq. (A13).

Here, the noninteracting term $H_0^{\mu_1}$ has the eigenvalues and eigenvectors as

$$\begin{aligned}
-2\Delta-\frac{\Gamma}{2}+\frac{\mu_1}{2}:&\quad \frac{1}{\sqrt{2}}(1\quad 1\quad 0\quad 0\quad 0\quad 0\quad 0\quad 0)^{\mathsf{T}},\\
-2\Delta+\frac{\Gamma}{2}+\frac{\mu_1}{2}:&\quad \frac{1}{\sqrt{2}}(-1\quad 1\quad 0\quad 0\quad 0\quad 0\quad 0\quad 0)^{\mathsf{T}},\\
2\Delta-\frac{\Gamma}{2}+\frac{\mu_1}{2}:&\quad \frac{1}{\sqrt{2}}(0\quad 0\quad -1\quad 1\quad 0\quad 0\quad 0\quad 0)^{\mathsf{T}},\\
2\Delta+\frac{\Gamma}{2}+\frac{\mu_1}{2}:&\quad \frac{1}{\sqrt{2}}(0\quad 0\quad 1\quad 1\quad 0\quad 0\quad 0\quad 0)^{\mathsf{T}},\\
\frac{\mu_1}{2}:&\quad \frac{1}{\sqrt{2}}(0\quad 0\quad 0\quad 0\quad 1\quad 0\quad 1\quad 0)^{\mathsf{T}},\\
\frac{\mu_1}{2}:&\quad \frac{1}{\sqrt{2}}(0\quad 0\quad 0\quad 0\quad 0\quad -1\quad 0\quad 1)^{\mathsf{T}},\\
-\Gamma+\frac{\mu_1}{2}:&\quad \frac{1}{2}(0\quad 0\quad 0\quad 0\quad 1\quad 1\quad -1\quad 1)^{\mathsf{T}},\\
\Gamma+\frac{\mu_1}{2}:&\quad \frac{1}{2}(0\quad 0\quad 0\quad 0\quad -1\quad 1\quad 1\quad 1)^{\mathsf{T}}.
\end{aligned}\tag{C4}$$

With the initial state $|ee\rangle=(1\quad 0\quad 0\quad 0\quad 0\quad 0\quad 0\quad 0)^{\mathsf{T}}$, the (unnormalized) final state in the Schrödinger picture is

$$\psi^{\mu_1}(\tau)=\begin{pmatrix}
e^{i\tau(2\Delta-\frac{\mu_1}{2})}\cos\left(\frac{\tau\Gamma}{2}\right)\\
ie^{i\tau(2\Delta-\frac{\mu_1}{2})}\sin\left(\frac{\tau\Gamma}{2}\right)\\
\frac{\Gamma}{4\Delta}e^{-\frac{i\tau\mu_1}{2}}\sin(2\tau\Delta)\sin\left(\frac{\tau\Gamma}{2}\right)\\
\frac{i\Gamma}{4\Delta}e^{-\frac{i\tau\mu_1}{2}}\sin(2\tau\Delta)\cos\left(\frac{\tau\Gamma}{2}\right)\\
\frac{1}{2}\mu_1 e^{i\tau(\Delta-\frac{\mu_1}{2})}\sin\left(\frac{\tau\Gamma}{2}\right)\left[\frac{1}{E_-}e^{\frac{i\tau\Gamma}{4}}\sin\left(\frac{E_-\tau}{2}\right)-\frac{1}{E_+}e^{-\frac{i\tau\Gamma}{4}}\sin\left(\frac{E_+\tau}{2}\right)\right]\\
\frac{1}{2}\mu_1 e^{i\tau(\Delta-\frac{\mu_1}{2})}\cos\left(\frac{\tau\Gamma}{2}\right)\left[-\frac{1}{E_-}ie^{\frac{i\tau\Gamma}{4}}\sin\left(\frac{E_-\tau}{2}\right)+\frac{1}{E_+}ie^{-\frac{i\tau\Gamma}{4}}\sin\left(\frac{E_+\tau}{2}\right)\right]\\
\frac{1}{2}\mu_1 e^{i\tau(\Delta-\frac{\mu_1}{2})}\cos\left(\frac{\tau\Gamma}{2}\right)\left[\frac{1}{E_-}ie^{\frac{i\tau\Gamma}{4}}\sin\left(\frac{E_-\tau}{2}\right)+\frac{1}{E_+}ie^{-\frac{i\tau\Gamma}{4}}\sin\left(\frac{E_+\tau}{2}\right)\right]\\
\frac{1}{2}\mu_1 e^{i\tau(\Delta-\frac{\mu_1}{2})}\sin\left(\frac{\tau\Gamma}{2}\right)\left[\frac{1}{E_-}e^{\frac{i\tau\Gamma}{4}}\sin\left(\frac{E_-\tau}{2}\right)+\frac{1}{E_+}e^{-\frac{i\tau\Gamma}{4}}\sin\left(\frac{E_+\tau}{2}\right)\right]
\end{pmatrix},\tag{C5}$$

where $E_\pm=2\Delta\pm\Gamma/2$.

Therefore, the leakage to the $|e'e'\rangle$ and $|o'o'\rangle$ is the same,

$$P_{e'e'}(\tau)+P_{o'o'}(\tau)=|\langle e'e'|\psi^{\mu_1}(\tau)\rangle|^2+|\langle o'o'|\psi^{\mu_1}(\tau)\rangle|^2=\frac{\Gamma^2\sin^2(2\tau\Delta)}{16\Delta^2},\tag{C6}$$

and the leakage to $|ee'\rangle$, $|oo'\rangle$, $|e'e\rangle$, and $|o'o\rangle$ is

$$\begin{aligned}
P_{ee'}(\tau)+P_{oo'}(\tau)+P_{e'e}(\tau)+P_{o'o}(\tau)&=|\langle ee'|\psi^{\mu_1}(\tau)\rangle|^2+|\langle oo'|\psi^{\mu_1}(\tau)\rangle|^2+|\langle e'e|\psi^{\mu_1}(\tau)\rangle|^2+|\langle o'o|\psi^{\mu_1}(\tau)\rangle|^2\\
&=\frac{\mu_1^2}{2}\left(\frac{\sin^2\left(\frac{E_-\tau}{2}\right)}{E_-^2}+\frac{\sin^2\left(\frac{E_+\tau}{2}\right)}{E_+^2}\right).
\end{aligned}\tag{C7}$$

This introduces a superposition of two frequencies E_- and E_+ in the leakage frequency, where the envelope frequency is $E_-+E_+=4\Delta$ and the carrier frequency is $E_+-E_-=\Gamma$.

APPENDIX D: LEAKAGE DUE TO μ_2

The leakage effect in the other on-site chemical potential is μ_2 (or μ_3). Namely, we set $\mu_1=\mu_3=\mu_4=0$, and $t=\Delta$. This leads to the same noninteracting part $H_0^{\mu_2}=H_0^{\mu_1}$ as in Eq. (C1), while the perturbation term $H_1^{\mu_2}$ is

$$H_1^{\mu_2}=\begin{pmatrix}H_1 & h_{\mu_2}\\ h_{\mu_2}^\dagger & 0\end{pmatrix},\tag{D1}$$

where H_1 is in Eq. (B2) and h_{μ_2} is

$$h_{\mu_2} = \frac{1}{2}\begin{pmatrix} 0 & 0 & -\mu_2 & 0 \\ 0 & 0 & 0 & -\mu_2 \\ -\mu_2 & 0 & 0 & 0 \\ 0 & -\mu_2 & 0 & 0 \end{pmatrix}. \tag{D2}$$

Here, the noninteracting term $H_0^{\mu_2}$ has the same eigenvalues (with μ_1 replaced with μ_2) and eigenvectors as in Eq. (C4), and, therefore, the final state in the Schrödinger picture starting from $|ee\rangle$ is

$$\psi^{\mu_2}(\tau) = \begin{pmatrix} e^{i\tau(2\Delta-\frac{\mu_2}{2})}\cos\left(\frac{\tau\Gamma}{2}\right) \\ ie^{i\tau(2\Delta-\frac{\mu_2}{2})}\sin\left(\frac{\tau\Gamma}{2}\right) \\ \frac{\Gamma}{4\Delta}e^{-\frac{i\tau\mu_2}{2}}\sin(2\tau\Delta)\sin\left(\frac{\tau\Gamma}{2}\right) \\ \frac{i\Gamma}{4\Delta}e^{-\frac{i\tau\mu_2}{2}}\sin(2\tau\Delta)\cos\left(\frac{\tau\Gamma}{2}\right) \\ \frac{\mu_2}{4}e^{i\tau(\Delta-\frac{\mu_2}{2})}\left[\left(\frac{i\sin\left(\frac{E_-\tau}{2}\right)}{E_-}-\frac{i\sin\left(\frac{E'_+\tau}{2}\right)}{E'_+}\right)e^{-\frac{i\tau\Gamma}{4}}+\left(-\frac{i\sin\left(\frac{E'_-\tau}{2}\right)}{E'_-}+\frac{i\sin\left(\frac{E_+\tau}{2}\right)}{E_+}\right)e^{\frac{i\tau\Gamma}{4}}\right] \\ \frac{\mu_2}{4}e^{i\tau(\Delta-\frac{\mu_2}{2})}\left[\left(\frac{i\sin\left(\frac{E_-\tau}{2}\right)}{E_-}+\frac{i\sin\left(\frac{E'_+\tau}{2}\right)}{E'_+}\right)e^{-\frac{i\tau\Gamma}{4}}+\left(-\frac{i\sin\left(\frac{E'_-\tau}{2}\right)}{E'_-}-\frac{i\sin\left(\frac{E_+\tau}{2}\right)}{E_+}\right)e^{\frac{i\tau\Gamma}{4}}\right] \\ \frac{\mu_2}{4}e^{i\tau(\Delta-\frac{\mu_2}{2})}\left[\left(\frac{i\sin\left(\frac{E_-\tau}{2}\right)}{E_-}+\frac{i\sin\left(\frac{E'_+\tau}{2}\right)}{E'_+}\right)e^{-\frac{i\tau\Gamma}{4}}+\left(\frac{i\sin\left(\frac{E'_-\tau}{2}\right)}{E'_-}+\frac{i\sin\left(\frac{E_+\tau}{2}\right)}{E_+}\right)e^{\frac{i\tau\Gamma}{4}}\right] \\ \frac{\mu_2}{4}e^{i\tau(\Delta-\frac{\mu_2}{2})}\left[\left(-\frac{i\sin\left(\frac{E_-\tau}{2}\right)}{E_-}+\frac{i\sin\left(\frac{E'_+\tau}{2}\right)}{E'_+}\right)e^{-\frac{i\tau\Gamma}{4}}+\left(-\frac{i\sin\left(\frac{E'_-\tau}{2}\right)}{E'_-}+\frac{i\sin\left(\frac{E_+\tau}{2}\right)}{E_+}\right)e^{\frac{i\tau\Gamma}{4}}\right] \end{pmatrix}, \tag{D3}$$

where $E_\pm = 2\Delta \pm \Gamma/2$ and $E'_\pm = 2\Delta \pm 3\Gamma/2$.

Therefore, the leakage to the $|e'e'\rangle$ and $|o'o'\rangle$ is the same as Eq. (C7), and the leakage to $|ee'\rangle$, $|oo'\rangle$, $|e'e\rangle$, and $|o'o\rangle$ is

$$\begin{aligned} P_{ee'}(\tau)+P_{oo'}(\tau)+P_{e'e}(\tau)+P_{o'o}(\tau) &= |\langle ee'|\psi^{\mu_2}(\tau)\rangle|^2+|\langle oo'|\psi^{\mu_2}(\tau)\rangle|^2+|\langle e'e|\psi^{\mu_2}(\tau)\rangle|^2+|\langle o'o|\psi^{\mu_2}(\tau)\rangle|^2 \\ &= \frac{\mu_2^2}{4}\left(\frac{\sin^2\left(\frac{E_-\tau}{2}\right)}{E_-^2}+\frac{\sin^2\left(\frac{E_+\tau}{2}\right)}{E_+^2}+\frac{\sin^2\left(\frac{E'_-\tau}{2}\right)}{{E'_-}^2}+\frac{\sin^2\left(\frac{E'_+\tau}{2}\right)}{{E'_+}^2}\right). \end{aligned} \tag{D4}$$

APPENDIX E: DEPHASING DUE TO DISORDER IN Γ

In this Appendix, we consider the dephasing effect which is used to estimate T_2. To focus only on the low-energy sector, we work in the minimal two-level system where the Hilbert space only includes $|ee\rangle$ and $|oo\rangle$. The effect of Γ acts like the magnetic field along the x direction and, therefore, the effective two-level Hamiltonian is

$$H_x = B_x\sigma_x, \tag{E1}$$

where B_x is quasistatic disorder following the Gaussian distribution with the variance of $\sigma_{B_x}^2$ and mean of $\bar{B}_x$, i.e., $B_x \sim \mathcal{N}(\bar{B}_x, \sigma_{B_x}^2)$, σ_x is the Pauli X matrix, and the initial state is $\psi_x(\tau=0) = |ee\rangle$.

Under the evolution of H_x, the final state $\psi_x(\tau)$ is

$$\psi_x(\tau) = e^{-iH_x\tau}\psi_x(\tau=0) = \begin{pmatrix} \cos(B_x\tau) \\ -i\sin(B_x\tau) \end{pmatrix}. \tag{E2}$$

Therefore, the probability of finding the state in $|oo\rangle$ is

$$P_{oo}(\tau) = |\langle oo|\psi_x(\tau)\rangle|^2 = \sin^2(B_x\tau). \tag{E3}$$

Thus, the disorder-averaged probability is

$$\begin{aligned} \langle P_{oo}(\tau)\rangle_{B_x} &= \frac{1}{\sqrt{2\pi}\sigma_{B_x}}\int_{-\infty}^{\infty} dB_x e^{-\frac{(B_x-\bar{B}_x)^2}{2\sigma_{B_x}^2}}\sin^2(B_x\tau) \\ &= \frac{1}{2}[1+e^{-2\tau^2\sigma_{B_x}^2}\cos(2\bar{B}_x\tau)]. \end{aligned} \tag{E4}$$

Therefore, the decay of the envelope of $\langle P_{oo}(\tau)\rangle_{B_x}$ follows the Gaussian decay with a prefactor of $e^{-2\tau^2\sigma_{B_x}^2}$, namely, $\beta = 2$ in the ansatz in Eq. (5) in the main text. This provides a fundamental understanding of the ansatz in Eq. (5) in the main text.

APPENDIX F: DEPHASING DUE TO DISORDER IN μ_i, Δ, AND t

Besides the dephasing effect due to the disorder in Γ, we also consider the dephasing effect due to the disorder in μ_i, Δ, and t.

In practice, the disorder of these quantities acts like the magnetic field along the z direction and, therefore, the effective two-level Hamiltonian is

$$H_{xz} = B_x\sigma_x + B_z\sigma_z, \tag{F1}$$

where B_x here is constant, B_z is quasistatic disorder following the Gaussian distribution with the variance of $\sigma_{B_z}^2$ and mean of 0, i.e., $B_z \sim \mathcal{N}(0, \sigma_{B_z}^2)$, σ_z is the Pauli Z matrix, and the initial state is again $\psi_{xz}(\tau = 0) = |ee\rangle$.

Under the evolution of H_{xz}, the final state $\psi_{xz}(\tau)$ is

$$\psi_{xz}(\tau) = e^{-iH_{xz}\tau}\psi_{xz}(\tau = 0) = \begin{pmatrix} \cos\left(\sqrt{B_x^2 + B_z^2}\tau\right) - i\sin\left(\sqrt{B_x^2 + B_z^2}\tau\right)\cos(\theta) \\ -i\sin\left(\sqrt{B_x^2 + B_z^2}\tau\right)\sin(\theta) \end{pmatrix}, \tag{F2}$$

where $\tan\theta = B_x/B_z$, and the probability of finding the state in $|oo\rangle$ is

$$P_{oo}(\tau) = |\langle oo|\psi_{xz}(\tau)\rangle|^2 = \sin^2\left(\sqrt{B_x^2 + B_z^2}\tau\right)\frac{B_x^2}{B_x^2 + B_z^2}. \tag{F3}$$

Therefore, the disorder-averaged probability is

$$\begin{aligned} &\langle P_{oo}(\tau)\rangle_{B_z} \\ &= \frac{1}{\sqrt{2\pi}\sigma_{B_z}}\int_{-\infty}^{\infty} dB_z e^{-\frac{B_z^2}{2\sigma_{B_z}^2}} \sin^2\left(\sqrt{B_x^2 + B_z^2}\tau\right)\frac{B_x^2}{B_x^2 + B_z^2} \\ &\approx \frac{1}{\sqrt{2\pi}\sigma_{B_z}}\int_{-\infty}^{\infty} dB_z e^{-\frac{B_z^2}{2\sigma_{B_z}^2}} \sin^2\left[\left(B_x^2 + \frac{B_z^2}{2B_x}\right)\tau\right] \\ &= \frac{1}{4}\left(2 - \frac{B_x e^{2iB_x\tau}}{\sqrt{B_x\left(B_x - 2i\sigma_{B_z}^2\tau\right)}} - \frac{B_x e^{-2iB_x\tau}}{\sqrt{B_x\left(B_x + 2i\sigma_{B_z}^2\tau\right)}}\right), \end{aligned} \tag{F4}$$

where the second line assumes the $B_z \ll B_x$ such that $\sqrt{B_x^2 + B_z^2} \approx B_x + \frac{B_z^2}{2B_x}$, and $\frac{B_x^2}{B_x^2 + B_z^2} \approx 1$. Therefore, it shows a power-law decay with $\langle P_{oo}(\tau)\rangle_{B_z} \sim \tau^{-\frac{1}{2}}$.

We provide the parameter for the numerical simulations of qubit dephasing in Figs. 3(d)–3(f). For the charge qubit in Fig. 3(d), we set $\varepsilon_{L/R} \sim \mathcal{N}(0, 3^2)$, $\Gamma_{L/R} \sim \mathcal{N}(5, 0.05^2)$ during the x pulse (i.e., with finite $\Gamma_{L/R}$) in units of meV, where $\mathcal{N}(\mu, \sigma^2)$ is the normal distribution with mean μ and variance σ^2; during the z pulse (i.e., with finite $\varepsilon_{L/R}$), we set $\varepsilon_L \sim \mathcal{N}(20, 3^2)$, $\varepsilon_R \sim \mathcal{N}(-20, 3^2)$, $\Gamma_{L/R} \sim \mathcal{N}(0, 0.05^2)$ in units of meV. For the small-gap Majorana qubit (all four $\Delta_{1,2,3,4} = 12$ meV) as shown in Fig. 3(e), during the x pulse, we set four $\mu_{1,2,3,4} \sim \mathcal{N}(0, 3^2)$, $t_{L/R} \sim \mathcal{N}(12, 0.016^2)$, and $\Gamma = 0.5$ meV; during the z pulse, we set four $\mu_{1,2,3,4} \sim \mathcal{N}(0, 3^2)$, $t_L \sim \mathcal{N}(14, 0.016^2)$, $t_R \sim \mathcal{N}(12, 0.016^2)$, and $\Gamma = 0$ meV. For the large-gap Majorana qubit (all four $\Delta_{1,2,3,4} = 38$ meV) as shown in Fig. 3(f), during the x pulse, we set four $\mu_{1,2,3,4} \sim \mathcal{N}(0, 0.3^2)$, $t_{L/R} \sim \mathcal{N}(38, 0.016^2)$, and $\Gamma = 0.5$ meV; during the z pulse, we set four $\mu_{1,2,3,4} \sim \mathcal{N}(0, 0.3^2)$, $t_L \sim \mathcal{N}(40, 0.016^2)$, $t_R \sim \mathcal{N}(38, 0.016^2)$, and $\Gamma = 0$ meV.

APPENDIX G: QUANTUM CAPACITANCE MEASUREMENT OF A MAJORANA QUBIT

In this Appendix, we show that the quantum capacitance measurement is capable of reading out $|ee\rangle$ and $|oo\rangle$ in a Majorana qubit. We first review the calculations in a single Kitaev chain, and then generalize it to a Majorana qubit composed of double Kitaev chains. The zero-temperature quantum capacitance of a state is defined as

$$C_q = -\frac{\partial^2 E}{\partial V_g^2}, \tag{G1}$$

where E is the eigenenergy of the state and V_g is the gate voltage. The Hamiltonian of a minimal Kitaev chain can be decomposed into even- and odd-parity sectors due to Fermi parity conservation. The even-parity Hamiltonian is

$$H_{\text{even}} = \begin{pmatrix} |00\rangle \\ |11\rangle \end{pmatrix}^T \begin{pmatrix} 0 & \Delta \\ \Delta & \mu_1 + \mu_2 \end{pmatrix}\begin{pmatrix} \langle 00| \\ \langle 11| \end{pmatrix}, \tag{G2}$$

where $\mu_{1,2}$ are the on-site energies of the two dots and t, Δ are the normal and Andreev couplings. The ground-state energy E_e of $|e\rangle$ is

$$E_e = \frac{\mu_1 + \mu_2}{2} - \sqrt{\Delta^2 + \left(\frac{\mu_1 + \mu_2}{2}\right)^2}. \tag{G3}$$

On the other hand, the derivative with respect to gate voltage is

$$\frac{\partial}{\partial V_g} = \alpha_1\frac{\partial}{\partial \mu_1} + \alpha_2\frac{\partial}{\partial \mu_2} \approx \alpha\left(\frac{\partial}{\partial \mu_1} + \frac{\partial}{\partial \mu_2}\right), \tag{G4}$$

where $\alpha_i \equiv d\mu_i/dV_g$ is the lever arm, and here we assume that all dots share a similar value of lever arm α. Therefore, it is straightforward to obtain the quantum capacitance of the even-parity ground state as below,

$$C_q^e = -\frac{\partial^2 E_e}{\partial V_g^2} = \frac{\alpha^2}{\sqrt{\Delta^2 + \left(\frac{\mu_1+\mu_2}{2}\right)^2}} - \frac{\alpha^2(\mu_1 + \mu_2)^2}{4\left[\Delta^2 + \left(\frac{\mu_1+\mu_2}{2}\right)^2\right]^{3/2}}. \tag{G5}$$

At the sweet spot of $\mu_1 = \mu_2 = 0$, we have

$$C_q^e = \frac{\alpha^2}{\Delta}. \tag{G6}$$

On the other hand, the Hamiltonian in the odd-parity sector is

$$H_{\text{odd}} = \begin{pmatrix} |10\rangle \\ |01\rangle \end{pmatrix}^T \begin{pmatrix} \mu_1 & t \\ t & \mu_2 \end{pmatrix}\begin{pmatrix} \langle 10| \\ \langle 01| \end{pmatrix}, \tag{G7}$$

with the ground-state energy being

$$E_o = \frac{\mu_1 + \mu_2}{2} - \sqrt{t^2 + \left(\frac{\mu_1 - \mu_2}{2}\right)^2}. \tag{G8}$$

The corresponding quantum capacitance is

$$C_q^o = 0, \tag{G9}$$

due to the opposite signs of the coefficients in front of μ_1 and μ_2 in the term of $(\frac{\mu_1-\mu_2}{2})^2$.

We now generalize our calculations to the quantum capacitance of the double Kitaev chain system. The eigenenergies

of the ground states are simply the sum of the left and right chains, i.e.,

$$E_{ab} = E_{aL}(\mu_{L1}, \mu_{L2}) + E_{bR}(\mu_{R1}, \mu_{R2}), \tag{G10}$$

where a, b denotes the parity e, o. We note that the μ dependence of E is separable between the left and right chains, which indicates that $\partial/\partial V_g \to \alpha(\frac{\partial}{\partial \mu_{L1}} + \frac{\partial}{\partial \mu_{L2}})$ for the left chain energy, while $\partial/\partial V_g \to \alpha(\frac{\partial}{\partial \mu_{R1}} + \frac{\partial}{\partial \mu_{R2}})$ for the right one. Therefore, we have

$$C_q^{ab} = -\frac{\partial^2 E_{ab}}{\partial V_g^2} = -\frac{\partial^2 E_{aL}}{\partial V_g^2} - \frac{\partial^2 E_{bR}}{\partial V_g^2} = C_q^{aL} + C_q^{bR}, \tag{G11}$$

that is, the quantum capacitance of the state in the whole system is a sum of the value in each chain separately. We therefore have

$$\begin{aligned} C_q^{ee} &= \frac{\alpha^2}{\Delta_L} + \frac{\alpha^2}{\Delta_R}, \\ C_q^{oo} &= 0, \\ C_q^{eo} &= \frac{\alpha^2}{\Delta_L}, \\ C_q^{oe} &= \frac{\alpha^2}{\Delta_R}. \end{aligned} \tag{G12}$$

Therefore, one can distinguish between $|ee\rangle$ and $|oo\rangle$ states using the quantum capacitance measurement. Furthermore, the values of C_q for $|eo\rangle$ and $|oe\rangle$ are generally very different from the qubit states. Thus our method also provides a possible way to investigate the quasiparticle poisoning effect by analyzing the readout results of $|eo\rangle$ and $|oe\rangle$.

[1] N. Read and D. Green, Paired states of fermions in two dimensions with breaking of parity and time-reversal symmetries and the fractional quantum Hall effect, Phys. Rev. B **61**, 10267 (2000).

[2] A. Y. Kitaev, Unpaired Majorana fermions in quantum wires, Phys. Usp. **44**, 131 (2001).

[3] C. Nayak, S. H. Simon, A. Stern, M. Freedman, and S. Das Sarma, Non-Abelian anyons and topological quantum computation, Rev. Mod. Phys. **80**, 1083 (2008).

[4] J. Alicea, New directions in the pursuit of Majorana fermions in solid state systems, Rep. Prog. Phys. **75**, 076501 (2012).

[5] M. Leijnse and K. Flensberg, Introduction to topological superconductivity and Majorana fermions, Semicond. Sci. Technol. **27**, 124003 (2012).

[6] C. W. J. Beenakker, Search for Majorana fermions in superconductors, Annu. Rev. Condens. Matter Phys. **4**, 113 (2013).

[7] T. D Stanescu and S. Tewari, Majorana fermions in semiconductor nanowires: Fundamentals, modeling, and experiment, J. Phys.: Condens. Matter **25**, 233201 (2013).

[8] J.-H. Jiang and S. Wu, Non-Abelian topological superconductors from topological semimetals and related systems under the superconducting proximity effect, J. Phys.: Condens. Matter **25**, 055701 (2013).

[9] S. D. Sarma, M. Freedman, and C. Nayak, Majorana zero modes and topological quantum computation, npj Quantum Inf. **1**, 15001 (2015).

[10] S. R. Elliott and M. Franz, Colloquium: Majorana fermions in nuclear, particle, and solid-state physics, Rev. Mod. Phys. **87**, 137 (2015).

[11] M. Sato and S. Fujimoto, Majorana fermions and topology in superconductors, J. Phys. Soc. Jpn. **85**, 072001 (2016).

[12] M. Sato and Y. Ando, Topological superconductors: A review, Rep. Prog. Phys. **80**, 076501 (2017).

[13] R. M. Lutchyn, E. P. A. M. Bakkers, L. P. Kouwenhoven, P. Krogstrup, C. M. Marcus, and Y. Oreg, Majorana zero modes in superconductor–semiconductor heterostructures, Nat. Rev. Mater. **3**, 52 (2018).

[14] H. Zhang, D. E. Liu, M. Wimmer, and L. P. Kouwenhoven, Next steps of quantum transport in Majorana nanowire devices, Nat. Commun. **10**, 5128 (2019).

[15] K. Flensberg, F. von Oppen, and A. Stern, Engineered platforms for topological superconductivity and Majorana zero modes, Nat. Rev. Mater. **6**, 944 (2021).

[16] S. Das Sarma, In search of Majorana, Nat. Phys. **19**, 165 (2023).

[17] J. D. Sau and S. D. Sarma, Realizing a robust practical Majorana chain in a quantum-dot-superconductor linear array, Nat. Commun. **3**, 964 (2012).

[18] H. Pan and S. Das Sarma, Physical mechanisms for zero-bias conductance peaks in Majorana nanowires, Phys. Rev. Res. **2**, 013377 (2020).

[19] S. Ahn, H. Pan, B. Woods, T. D. Stanescu, and S. Das Sarma, Estimating disorder and its adverse effects in semiconductor Majorana nanowires, Phys. Rev. Mater. **5**, 124602 (2021).

[20] S. Das Sarma, J. D. Sau, and T. D. Stanescu, Spectral properties, topological patches, and effective phase diagrams of finite disordered Majorana nanowires, Phys. Rev. B **108**, 085416 (2023).

[21] S. Das Sarma and H. Pan, Density of states, transport, and topology in disordered Majorana nanowires, Phys. Rev. B **108**, 085415 (2023).

[22] J. R. Taylor, J. D. Sau, and S. Das Sarma, Machine learning the disorder landscape of Majorana nanowires, Phys. Rev. Lett. **132**, 206602 (2024).

[23] C.-X. Liu, G. Wang, T. Dvir, and M. Wimmer, Tunable superconducting coupling of quantum dots via Andreev bound states in semiconductor-superconductor nanowires, Phys. Rev. Lett. **129**, 267701 (2022).

[24] A. Bordin, G. Wang, C.-X. Liu, S. L. D. ten Haaf, N. van Loo, G. P. Mazur, D. Xu, D. van Driel, F. Zatelli, S. Gazibegovic, G. Badawy, E. P. A. M. Bakkers, M. Wimmer, L. P. Kouwenhoven, and T. Dvir, Tunable crossed Andreev reflection and elastic cotunneling in hybrid nanowires, Phys. Rev. X **13**, 031031 (2023).

[25] G. Wang, T. Dvir, G. P. Mazur, C.-X. Liu, N. van Loo, S. L. D. ten Haaf, A. Bordin, S. Gazibegovic, G. Badawy, E. P. A. M. Bakkers, M. Wimmer, and L. P. Kouwenhoven, Singlet and triplet Cooper pair splitting in hybrid superconducting nanowires, Nature (London) **612**, 448 (2022).

[26] Q. Wang, S. L. D. ten Haaf, I. Kulesh, D. Xiao, C. Thomas, M. J. Manfra, and S. Goswami, Triplet correlations in Cooper pair splitters realized in a two-dimensional electron gas, Nat. Commun. **14**, 4876 (2023).

[27] A. Bordin, X. Li, D. van Driel, J. C. Wolff, Q. Wang, S. L. D. ten Haaf, G. Wang, N. van Loo, L. P. Kouwenhoven, and T. Dvir, Crossed Andreev reflection and elastic cotunneling in three quantum dots coupled by superconductors, Phys. Rev. Lett. **132**, 056602 (2024).

[28] M. Leijnse and K. Flensberg, Parity qubits and poor man's Majorana bound states in double quantum dots, Phys. Rev. B **86**, 134528 (2012).

[29] T. Dvir, G. Wang, N. van Loo, C.-X. Liu, G. P. Mazur, A. Bordin, S. L. D. ten Haaf, J.-Y. Wang, D. van Driel, F. Zatelli, X. Li, F. K. Malinowski, S. Gazibegovic, G. Badawy, E. P. A. M. Bakkers, M. Wimmer, and L. P. Kouwenhoven, Realization of a minimal Kitaev chain in coupled quantum dots, Nature (London) **614**, 445 (2023).

[30] F. Zatelli, D. van Driel, D. Xu, G. Wang, C.-X. Liu, A. Bordin, B. Roovers, G. P. Mazur, N. van Loo, J. C. Wolff *et al.*, Robust poor man's Majorana zero modes using Yu-Shiba-Rusinov states, Nat. Commun. **15**, 7933 (2024).

[31] A. Bordin, C.-X. Liu, T. Dvir, F. Zatelli, S. L. ten Haaf, D. van Driel, G. Wang, N. van Loo, T. van Caekenberghe, J. C. Wolff *et al.*, Signatures of Majorana protection in a three-site Kitaev chain, arXiv:2402.19382.

[32] S. L. D. ten Haaf, Q. Wang, A. M. Bozkurt, C.-X. Liu, I. Kulesh, P. Kim, D. Xiao, C. Thomas, M. J. Manfra, T. Dvir, M. Wimmer, and S. Goswami, A two-site Kitaev chain in a two-dimensional electron gas, Nature (London) **630**, 329 (2024).

[33] J. D. Sau and S. D. Sarma, Capacitance-based fermion parity read-out and predicted Rabi oscillations in a Majorana nanowire, arXiv:2406.18080.

[34] C.-X. Liu, H. Pan, F. Setiawan, M. Wimmer, and J. D. Sau, Fusion protocol for Majorana modes in coupled quantum dots, Phys. Rev. B **108**, 085437 (2023).

[35] P. Boross and A. Pályi, Braiding-based quantum control of a Majorana qubit built from quantum dots, Phys. Rev. B **109**, 125410 (2024).

[36] A. Tsintzis, R. S. Souto, K. Flensberg, J. Danon, and M. Leijnse, Majorana qubits and non-Abelian physics in quantum dot–based minimal Kitaev chains, PRX Quantum **5**, 010323 (2024).

[37] V. Mourik, K. Zuo, S. M. Frolov, S. R. Plissard, E. P. A. M. Bakkers, and L. P. Kouwenhoven, Signatures of Majorana fermions in hybrid superconductor-semiconductor nanowire devices, Science **336**, 1003 (2012).

[38] F. Nichele, A. C. C. Drachmann, A. M. Whiticar, E. C. T. O'Farrell, H. J. Suominen, A. Fornieri, T. Wang, G. C. Gardner, C. Thomas, A. T. Hatke, P. Krogstrup, M. J. Manfra, K. Flensberg, and C. M. Marcus, Scaling of Majorana zero-bias conductance peaks, Phys. Rev. Lett. **119**, 136803 (2017).

[39] H. Zhang, M. W. A. de Moor, J. D. S. Bommer, D. Xu, G. Wang, N. van Loo, C.-X. Liu, S. Gazibegovic, J. A. Logan, D. Car *et al.*, Large zero-bias peaks in InSb-Al hybrid semiconductor-superconductor nanowire devices, arXiv:2101.11456.

[40] M. Aghaee, A. Akkala, Z. Alam, R. Ali, A. Alcaraz Ramirez, M. Andrzejczuk, A. E. Antipov, P. Aseev, M. Astafev, B. Bauer, J. Becker, S. Boddapati, F. Boekhout, J. Bommer, T. Bosma, L. Bourdet, S. Boutin, P. Caroff, L. Casparis, M. Cassidy, S. Chatoor, A. W. Christensen, N. Clay, W. S. Cole, F. Corsetti, A. Cui, P. Dalampiras, A. Dokania, G. de Lange, M. de Moor, J. C. Estrada Saldaña, S. Fallahi, Z. H. Fathabad, J. Gamble, G. Gardner, D. Govender, F. Griggio, R. Grigoryan, S. Gronin, J. Gukelberger, E. B. Hansen, S. Heedt, J. Herranz Zamorano, S. Ho, U. L. Holgaard, H. Ingerslev, L. Johansson, J. Jones, R. Kallaher, F. Karimi, T. Karzig, E. King, M. E. Kloster, C. Knapp, D. Kocon, J. Koski, P. Kostamo, P. Krogstrup, M. Kumar, T. Laeven, T. Larsen, K. Li, T. Lindemann, J. Love, R. Lutchyn, M. H. Madsen, M. Manfra, S. Markussen, E. Martinez, R. McNeil, E. Memisevic, T. Morgan, A. Mullally, C. Nayak, J. Nielsen, W. H. P. Nielsen, B. Nijholt, A. Nurmohamed, E. O'Farrell, K. Otani, S. Pauka, K. Petersson, L. Petit, D. I. Pikulin, F. Preiss, M. Quintero-Perez, M. Rajpalke, K. Rasmussen, D. Razmadze, O. Reentila, D. Reilly, R. Rouse, I. Sadovskyy, L. Sainiemi, S. Schreppler, V. Sidorkin, A. Singh, S. Singh, S. Sinha, P. Sohr, T. Stankevič, L. Stek, H. Suominen, J. Suter, V. Svidenko, S. Teicher, M. Temuerhan, N. Thiyagarajah, R. Tholapi, M. Thomas, E. Toomey, S. Upadhyay, I. Urban, S. Vaitiekėnas, K. Van Hoogdalem, D. Van Woerkom, D. V. Viazmitinov, D. Vogel, S. Waddy, J. Watson, J. Weston, G. W. Winkler, C. K. Yang, S. Yau, D. Yi, E. Yucelen, A. Webster, R. Zeisel, and R. Zhao(Microsoft Quantum), InAs-Al hybrid devices passing the topological gap protocol, Phys. Rev. B **107**, 245423 (2023).

[41] J. D. Sau, R. M. Lutchyn, S. Tewari, and S. Das Sarma, Generic new platform for topological quantum computation using semiconductor heterostructures, Phys. Rev. Lett. **104**, 040502 (2010).

[42] R. M. Lutchyn, J. D. Sau, and S. Das Sarma, Majorana fermions and a topological phase transition in semiconductor-superconductor heterostructures, Phys. Rev. Lett. **105**, 077001 (2010).

[43] Y. Oreg, G. Refael, and F. von Oppen, Helical liquids and Majorana bound states in quantum wires, Phys. Rev. Lett. **105**, 177002 (2010).

[44] X. Hu and S. Das Sarma, Charge-fluctuation-induced dephasing of exchange-coupled spin qubits, Phys. Rev. Lett. **96**, 100501 (2006).

[45] K. D. Petersson, J. R. Petta, H. Lu, and A. C. Gossard, Quantum coherence in a one-electron semiconductor charge qubit, Phys. Rev. Lett. **105**, 246804 (2010).

[46] O. E. Dial, M. D. Shulman, S. P. Harvey, H. Bluhm, V. Umansky, and A. Yacoby, Charge noise spectroscopy using coherent exchange oscillations in a singlet-triplet qubit, Phys. Rev. Lett. **110**, 146804 (2013).

[47] P. Scarlino, J. H. Ungerer, D. J. van Woerkom, M. Mancini, P. Stano, C. Müller, A. J. Landig, J. V. Koski, C. Reichl, W. Wegscheider, T. Ihn, K. Ensslin, and A. Wallraff, *In situ* tuning of the electric-dipole strength of a double-dot charge qubit: Charge-noise protection and ultrastrong coupling, Phys. Rev. X **12**, 031004 (2022).

[48] E. J. Connors, J. Nelson, L. F. Edge, and J. M. Nichol, Charge-noise spectroscopy of Si/SiGe quantum dots via dynamically-decoupled exchange oscillations, Nat. Commun. **13**, 940 (2022).

[49] R. E. Throckmorton and S. Das Sarma, Crosstalk- and charge-noise-induced multiqubit decoherence in exchange-coupled quantum dot spin qubit arrays, Phys. Rev. B **105**, 245413 (2022).

[50] G. Burkard, T. D. Ladd, A. Pan, J. M. Nichol, and J. R. Petta, Semiconductor spin qubits, Rev. Mod. Phys. **95**, 025003 (2023).

[51] E. Paladino, Y. M. Galperin, G. Falci, and B. L. Altshuler, $1/f$ noise: Implications for solid-state quantum information, Rev. Mod. Phys. **86**, 361 (2014).

[52] G. Ithier, E. Collin, P. Joyez, P. J. Meeson, D. Vion, D. Esteve, F. Chiarello, A. Shnirman, Y. Makhlin, J. Schriefl, and G. Schön, Decoherence in a superconducting quantum bit circuit, Phys. Rev. B **72**, 134519 (2005).

[53] P. Boross and A. Pályi, Dephasing of Majorana qubits due to quasistatic disorder, Phys. Rev. B **105**, 035413 (2022).

[54] T. Hayashi, T. Fujisawa, H. D. Cheong, Y. H. Jeong, and Y. Hirayama, Coherent manipulation of electronic states in a double quantum dot, Phys. Rev. Lett. **91**, 226804 (2003).

[55] C.-X. Liu, A. M. Bozkurt, F. Zatelli, S. L. D. ten Haaf, T. Dvir, and M. Wimmer, Enhancing the excitation gap of a quantum-dot-based Kitaev chain, Commun. Phys. **7**, 235 (2024).

[56] Y. Luh, Bound state in superconductors with paramagnetic impurities, Acta Phys. Sin. **21**, 75 (1965).

[57] H. Shiba, Classical spins in superconductors, Prog. Theor. Phys. **40**, 435 (1968).

[58] A. Rusinov, Theory of gapless superconductivity in alloys containing paramagnetic impurities, Sov. Phys. JETP **29**, 1101 (1969).

[59] M. Aghaee, A. A. Ramirez, Z. Alam, R. Ali, M. Andrzejczuk, A. Antipov, M. Astafev, A. Barzegar, B. Bauer, J. Becker *et al.*, Interferometric single-shot parity measurement in an inas-al hybrid device, arXiv:2401.09549.

[60] C.-X. Liu, S. Miles, A. Bordin, S. L. D. ten Haaf, A. M. Bozkurt, and M. Wimmer, Protocol for scaling up a sign-ordered Kitaev chain without magnetic flux control, arXiv:2407.04630.

Editors' Suggestion

Rabi and Ramsey oscillations of a Majorana qubit in a quantum dot-superconductor array

Haining Pan [1], Sankar Das Sarma,[2] and Chun-Xiao Liu [3,*]

[1]*Department of Physics and Astronomy, Center for Materials Theory, Rutgers University, Piscataway, New Jersey 08854, USA*

[2]*Condensed Matter Theory Center and Joint Quantum Institute, Department of Physics, University of Maryland, College Park, Maryland 20742, USA*

[3]*QuTech and Kavli Institute of NanoScience, Delft University of Technology, Delft, The Netherlands*

(Received 31 July 2024; revised 20 January 2025; accepted 27 January 2025; published 12 February 2025)

The Kitaev chain can be engineered within a quantum dot-superconductor array, hosting Majorana zero modes at fine-tuned sweet spots. In this work, we propose and simulate the occurrence of Rabi and Ramsey oscillations to feasibly construct a minimal Majorana qubit in the quantum dot setup. Our real-time results incorporate realistic effects, e.g., charge noise and leakage, reflecting the latest experimental progress. We demonstrate that Majorana qubits with larger energy gaps exhibit significantly enhanced performance—longer dephasing times, higher quality factors, reduced leakage probabilities, and improved visibilities—compared to those with smaller gaps and with conventional quantum-dot-based charge qubits. We introduce a method for reading out Majorana qubits via quantum capacitance measurements. Our work paves the way for future experiments on realizing Majorana qubits in quantum dot-superconductor arrays.

DOI: 10.1103/PhysRevB.111.075416

I. INTRODUCTION

Majorana zero modes are non-Abelian anyonic excitations localized at the defects or edges of a topological superconductor [1–16]. Qubits constructed from the Majorana excitations are immune to local noise and are fault tolerant without active error corrections, offering a pathway to implementing error-resilient topological quantum computing [3,9]. Recently, the quantum dot-superconductor array has become a promising candidate for realizing topological Kitaev chains [2] in solid-state physics using a concrete idea proposed a while ago [17]. An advantage of this quantum-dot-based approach is the intrinsic robustness against the effect of disorder that is ubiquitous in semiconductor-superconductor Majorana platforms [18–22]. In addition, utilizing Andreev bound states in a hybrid region as the coupler enables precise control over the relative amplitudes of normal and superconducting interactions between quantum dots [23–27], thus allowing for fine tuning of a quantum dot-superconductor array into a sweet spot with optimally protected Majorana zero modes [2,17,28]. Tunnel spectroscopic signatures of Majoranas have been observed in recent experiments on quantum dots using both nanowires [29–31] and two-dimensional electrons [32].

To decisively establish a Majorana qubit and demonstrate its topologically enhanced coherence, Rabi oscillation experiments on quantum-dot-based Kitaev chains are necessary [33]. Additionally, understanding the topological coherence and obtaining a sufficiently long coherence time is crucial for detecting the non-Abelian statistics of Majorana anyons in fusion [34] or braiding [35,36] experiments. Most importantly (and as we demonstrate in the current work), such a Rabi oscillation experiment is already feasible in currently available platforms [29–32], provided that two such minimal Kitaev chains are interconnected via a common superconducting lead and are normal tunnel coupled at their ends [see Fig. 1(a)].

In the current work, we propose Rabi and Ramsey oscillation experiments in a minimal Majorana qubit composed of double two-site Kitaev chains [see Fig. 1(a)]. Our real-time simulations incorporate realistic effects such as charge noise and leakage to the noncomputational bases. We find that Majorana qubits constructed from large-gap Kitaev chains significantly outperform those with smaller gaps and conventional quantum-dot-based charge qubits in terms of dephasing time, quality factor, leakage probability, and visibility. In addition, we propose a Majorana qubit readout method based on quantum capacitance. Our work demonstrates the optimal route to the first step of establishing a Majorana qubit as a viable experimental entity, which has not been achieved in the 15 years of experiments [37–40] and 25 years of theory [1–3,41–43] on topological quantum computing.

II. SETUP AND HAMILTONIAN

A minimal Majorana qubit consists of double two-site Kitaev chains, as shown in Fig. 1(a). The Hamiltonian is

$$\begin{aligned}\mathcal{H}_{\rm tot} &= \mathcal{H}_L + \mathcal{H}_R + \mathcal{H}_{\rm tunn},\\ \mathcal{H}_a &= \sum_{i=1}^{2} \mu_{ai} n_{ai} + (t_a c_{a2}^\dagger c_{a1} + \Delta_a c_{a2} c_{a1} + \text{H.c.}),\\ \mathcal{H}_{\rm tunn} &= \Gamma c_{R1}^\dagger c_{L2} + \text{H.c.}\end{aligned} \tag{1}$$

Here, $\mathcal{H}_a$ with $a \in \{L, R\}$ is the Hamiltonian for the left and right chain, respectively, with μ_{ai} $(i = 1, 2)$ the on-site

*Contact author: chunxiaoliu62@gmail.com

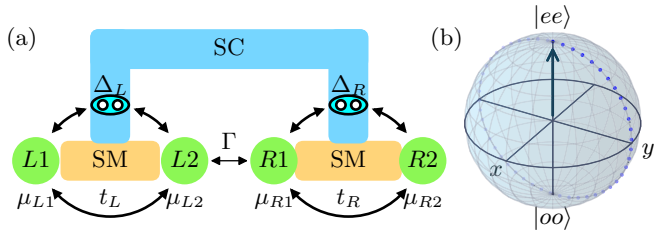

FIG. 1. (a) Schematic of a Majorana qubit composed of double two-site Kitaev chains. (b) Bloch sphere. $|\pm z\rangle$ are defined as $|ee\rangle$ and $|oo\rangle$, respectively. The dots represent the trajectory of the state vector in a Rabi experiment.

energy of a spin-polarized dot orbital, $n_{ai} = c_{ai}^\dagger c_{ai} = 0, 1$ the occupancy number, and t_a and Δ_a the strengths of the normal and Andreev tunnelings. $H_{\rm tunn}$ is the tunnel Hamiltonian, with Γ being the strength of single-electron transfer between dots from different chains. In the current work, we are particularly interested in the sweet spot of the system, which is defined as $\mu_{ai} = 0$ and $t_a = \Delta_a$. Although Δ_L and Δ_R can be different in strength, in the current work we assume them to be equal to simplify the discussions. At that point, the even-parity ground state $|e\rangle_a = (|00\rangle_a - |11\rangle_a)/\sqrt{2}$ is degenerate with the odd-parity one $|o\rangle_a = (|10\rangle_a - |01\rangle_a)/\sqrt{2}$ within each Kitaev chain, hosting a pair of Majorana zero modes at two separate quantum dots. Here, $|n_1 n_2\rangle_a = (c_{a1}^\dagger)^{n_1}(c_{a2}^\dagger)^{n_2}|0\rangle_a$, and $|0\rangle_a$ is the vacuum state of chain a. Since total fermion parity is conserved in the Hamiltonian of Eq. (1), we can focus on the subspace with total parity even without loss of generality. As such, the ground-state degeneracy is twofold,

$$|ee\rangle \equiv |e\rangle_L \otimes |e\rangle_R, \quad |oo\rangle \equiv |o\rangle_L \otimes |o\rangle_R, \tag{2}$$

which form the basis states of a Majorana qubit.

Rabi oscillations. In the qubit subspace spanned by $|ee\rangle$ and $|oo\rangle$, the low-energy effective Hamiltonian is

$$H_{\rm eff} = \frac{\varepsilon}{2}\sigma_z + \frac{\Gamma}{2}\sigma_x, \tag{3}$$

where $\varepsilon \equiv E_{oo} - E_{ee}$ and $\sigma_{x/z}$ are Pauli X/Z matrices. Here, σ_z rotation is proportional to the ground-state energy splitting, which we choose to be $\varepsilon = t_L - \Delta_L$ by detuning the hybrid region in the left chain away from the sweet spot [30]. σ_x rotation is realized by single-electron tunneling between the two chains that can be controlled by a tunnel barrier. Motivated by the form of $H_{\rm eff}$ in Eq. (3), we perform a numerical simulation of the Rabi and Ramsey experiments using the total Hamiltonian $\mathcal{H}_{\rm tot}$ in Eq. (1). Here we implement the qubit rotations by applying sequences of pulses of ε or Γ instead of microwave driving because of the basis state degeneracy. In particular, in the Rabi experiment, the system is initialized in $|ee\rangle$ of two decoupled Kitaev chains at their sweet spots. This corresponds to the north pole of the Bloch sphere. We then turn on the interchain tunneling Γ and let the system evolve for a time τ before performing a readout in the σ_z basis [see pulse profiles in Fig. 2(a)]. Figure 2(b) shows the numerically calculated $P_{ee}(\tau) \equiv |\langle ee|\psi(\tau)\rangle|^2$ in the (Γ, τ) plane. Indeed, the fringe pattern of Rabi oscillations confirms that single-electron tunneling $H_{\rm tunn}$ in Eq. (1) works as a σ_x rotation in the qubit subspace, with the oscillation frequency being

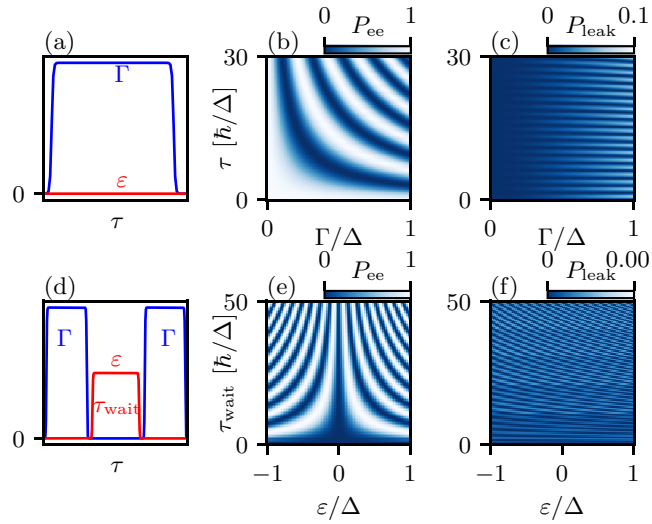

FIG. 2. Numerical simulations in the clean limit. Upper panels: Numerical simulation of a Rabi experiment. (a) Pulse profiles. (b), (c) P_{ee} and $P_{\rm leak}$ in Eq. (7) in the (Γ, τ) plane. Lower panels: Numerical simulation of a Ramsey experiment. (d) Pulse profiles. (e), (f) P_{ee} and $P_{\rm leak}$ in the $(\varepsilon, \tau_{\rm wait})$ plane. Here, $\Delta_L = \Delta_R = \Delta$.

proportional to Γ. However, surprisingly, we also find that the state wave function can leak out of the qubit subspace with a probability $P_{\rm leak}(\tau) \equiv 1 - P_{ee}(\tau) - P_{oo}(\tau)$, which oscillates periodically in time and increases with the tunneling strength Γ [see Fig. 2(c)]. Using time-dependent perturbation theory (see Appendix B), we show that a finite interchain tunneling Γ inevitably induces a leakage to the excited states of $|e'e'\rangle$ and $|o'o'\rangle$, i.e.,

$$P_{\rm leak}(\tau) = P_{e'e'}(\tau) + P_{o'o'}(\tau) \approx \frac{\Gamma^2}{16\Delta^2}\sin^2(2\Delta\tau/\hbar), \tag{4}$$

where $|e'\rangle_a = (|00\rangle_a + |11\rangle_a)/\sqrt{2}$ and $|o'\rangle_a = (|10\rangle_a + |01\rangle_a)/\sqrt{2}$ are excited states in each chain and $\Delta_L = \Delta_R = \Delta$. Here the oscillation frequency of the leakage probability is $4\Delta/\hbar$ and the magnitude scales with Γ^2/Δ^2. On the other hand, in a Ramsey experiment, we first apply a pulse of $H_{\rm tunn}$ to rotate the initial state $|ee\rangle$ to the equator of the Bloch sphere, then let it evolve for a time duration $\tau_{\rm wait}$ in the presence of a finite ε, and apply the same $H_{\rm tunn}$ pulse again before the final readout [see pulse profiles in Fig. 2(d)]. The simulated $P_{ee}(\tau)$ in the $(\varepsilon, \tau_{\rm wait})$ plane is shown in Fig. 2(e). Here the small $P_{\rm leak}$ in Fig. 2(f) is due to the σ_x pulses, while detuning the coupling $t_L - \Delta_L$ has a negligible impact on the leakage probability. Both experiments are doable in the currently available devices and provide complementary information about Majorana coherence.

III. QUBIT DEPHASING

Charge noise is one of the primary sources of decoherence in semiconductor-based qubits [44–51]. It can be induced by charge impurities in the environment or fluctuations in the nearby gate voltages. As a $1/f$ noise, the fluctuations are dominated by the low-frequency components, which can be modeled by the quasistatic disorder approximation, since

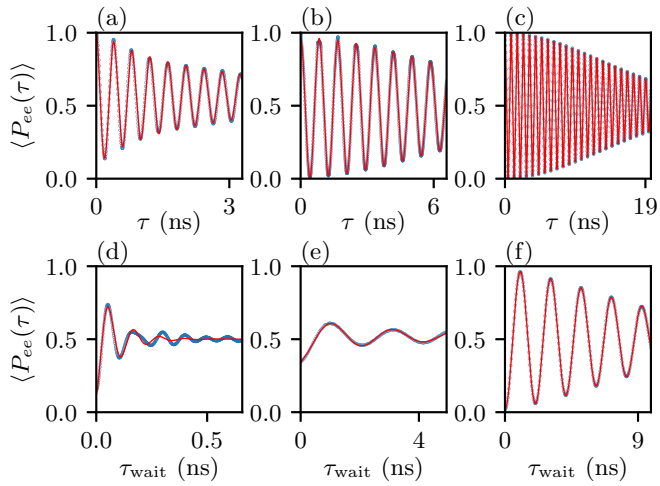

FIG. 3. Numerical simulations including charge noises. Upper panels: Rabi oscillations of disorder-averaged $\langle P_{ee}\rangle$. Lower panels: Ramsey oscillations of disorder-averaged $\langle P_{ee}\rangle$. (a), (d) Semiconductor charge qubits. (b), (e) Small-gap Majorana qubits. (c), (f) Large-gap Majorana qubits. The blue dots are data from numerical simulations, while the red lines are fitting curves using Eq. (5). Here, the size of the disorder ensemble is 500.

the zero-frequency part of the noise dominates [52,53]. That is, in each run of the Rabi or Ramsey experiment, the Hamiltonian parameters in Eq. (1) are subject to a static disorder that obeys normal distribution, and the final readout measurement is averaged over 500 different disorder realizations, giving $\langle P_{ee}(\tau)\rangle$. In particular, we simulate and compare three different types of qubits: (1) a semiconductor charge qubit with one electron in double quantum dots [51,54], (2) a small-gap Majorana qubit [29], and (3) a large-gap Majorana qubit [30,32]. Here a small (large) gap in the Kitaev chain corresponds to the scenario where the dot-hybrid coupling strength is smaller than (comparable to) the induced gap in the hybrid region [55]. The mean values and standard deviations of the Hamiltonian parameters that are subject to charge noises are chosen according to the values reported in relevant experimental works, which are summarized in the Appendix F. Figure 3 shows the calculated Rabi and Ramsey oscillations of $\langle P_{ee}(\tau)\rangle$ with dephasing for all three types of qubits. The curves with decaying envelopes are further fitted using the following formula:

$$\langle P_{ee}(\tau)\rangle = P_0 + A\cos(2\pi f\tau + \phi_0)\exp -(\tau/T_2)^{\beta}, \quad (5)$$

where $2A$ is the visibility, T_2 is the dephasing time, and β is the decaying exponent. Their values are summarized in Table I and, in addition, we define the quality factor as

$$Q = 2\pi f T_2, \quad (6)$$

and the leakage probability as

$$P_{\rm leak} = \lim_{\tau_0\to\infty}\int_0^{\tau_0}\langle P_{\rm leak}(\tau)\rangle d\tau/\tau_0, \quad (7)$$

in the long-time limit where $\langle P_{\rm leak}(\tau)\rangle = 1 - \langle P_{ee}(\tau)\rangle - \langle P_{oo}(\tau)\rangle$ is the instantaneous value.

The Hamiltonian for a semiconductor charge qubit is

$$H_c = \begin{pmatrix}\varepsilon_L & \Gamma\\ \Gamma & \varepsilon_R\end{pmatrix}, \quad (8)$$

where the basis states are $|10\rangle$ and $|01\rangle$ with one electron in the left or right quantum dot, ε_L (ε_R) is the corresponding orbital energy in the left (right) dot, and Γ is the interdot coupling strength. Here, the fluctuations of the dot energies σ_ε dominate the dephasing effect, compared to the fluctuations of the interdot coupling strength σ_Γ, due to the small magnitude of Γ. In the Rabi experiment, the dot energies are tuned into a sweet spot of $\varepsilon_L = \varepsilon_R = 0$, which is insensitive to dot-energy detuning up to the first order, i.e., $\partial E/\partial\varepsilon_a = 0$. However, since the dot-energy fluctuations are large and comparable to the interdot coupling strength, e.g., $\sigma_\varepsilon = 3$ μeV $\simeq$ $\Gamma = 5$ μeV, the higher-order contributions (e.g., $\delta E \sim \sigma_\varepsilon^2/\Gamma$) lead to a short dephasing time $T_2 \approx 2.50(7)$ ns for x rotations; see Fig. 3(a). In the Ramsey experiment, to implement the z rotation, we choose $\varepsilon_L = -\varepsilon_R = 20$ μeV $\gg \Gamma$, which is much more susceptible to charge noise as $\partial E/\partial\varepsilon_a \approx 1$. Thus, the dephasing time is even shorter, $T_2 \approx 0.096(2)$ ns, and the visibility is reduced; see Fig. 3(d). The consistency between our T_2 estimates and the experimental measurements reported in Ref. [54] validates our modeling of the quantum dot devices.

In a minimal two-site Kitaev chain that is in the vicinity of the sweet spot, the energy splitting between the even- and odd-parity ground states is approximately $E \equiv E_o - E_e \approx$

TABLE I. Comparison of qubit performances.

Protocol	Qubit properties	Charge qubit	Small-gap Majorana qubit	Large-gap Majorana qubit
Rabi	T_2 (ns) [Eq. (5)]	2.50(7)	9.25(5)	19.064(8)
	Q [Eq. (6)]	38(1)	69.4(4)	144.7(5)
	$2A$ [Eq. (5)]	1.01(2)	0.958(1)	1.001(3)
	$P_{\rm leak}$ [Eq. (7)]		0.035	$5.7(8)\times10^{-4}$
	β [Eq. (5)]	0.66(2)	1.87(2)	1.941(3)
Ramsey	T_2 (ns) [Eq. (5)]	0.096(2)	1.84(7)	11.23(1)
	Q [Eq. (6)]	5.3(2)	5.6(2)	34.31(3)
	$2A$ [Eq. (5)]	0.77(2)	0.3716(8)	0.950(5)
	$P_{\rm leak}$ [Eq. (7)]		0.0275(1)	$3.31(6)\times10^{-5}$
	β [Eq. (5)]	1.01(4)	0.57(2)	1.557(4)

$\mu_1\mu_2/2t + (t - \Delta)$, where the first term is due to the simultaneous detuning of on-site dot energies, while the second term is the detuning of the hybrid region. In a small-gap Majorana qubit (i.e., small $t \equiv \Delta$ limit), the dot-energy fluctuations are comparatively dominant, giving a characteristic energy splitting between the basis states $\delta E \sim \sigma_\mu^2/t$. For a Majorana qubit defined in Fig. 1(a), such a δE leads to noise in the σ_z basis. In the Rabi experiment, since the dot-energy noise ($\propto \sigma_z$) is orthogonal to the σ_x rotation, the dephasing effect of the dot-energy fluctuations is strongly mitigated (see the Appendix F). As such, $T_2 \approx 9.25(5)$ ns is jointly determined by the fluctuations in the dot energies ($\propto \sigma_z$) as well as in the interchain coupling strengths ($\propto \sigma_x$); see Fig. 3(b). In the Ramsey experiment on σ_z rotations, the large dot-energy fluctuations ($\propto \sigma_z$) cause a more detrimental effect on qubit dephasing, giving a much shorter dephasing time $T_2 \approx 1.84(7)$ ns and a reduced visibility $2A \approx 0.3716(8)$; see Fig. 3(e) and Table I. Note that here the dephasing effect of charge noise in t_a and Δ_a is negligible because of the weak dot-superconductor hybridization.

On the contrary, the performance of a large-gap Majorana qubit is much improved in almost all aspects, e.g., dephasing time, quality factor, visibility, and leakage probability. The strong dot-superconductor hybridization not only strongly enhances the excitation gap of a Kitaev chain, but also transforms the dot orbitals into Yu-Shiba-Rusinov states [56–58], thus significantly screening the electric charge in the quantum dots [30,32,55]. As a result, the energy splitting due to μ_{ai} fluctuations in the effective Kitaev chain is strongly suppressed, i.e., σ_μ^2/t is reduced by a factor of ∼300 compared to the small-gap Majorana qubit. Now the dominant source of dephasing in the Rabi experiment is the charge noise in Γ, giving $T_2 \approx 19.064(8)$ ns; see Fig. 3(c). In the Ramsey experiment, the fluctuations of $t_a - \Delta_a$ begin to dominate the dephasing, giving $T_2 \approx 11.23(1)$ ns; see Fig. 3(f). In addition, a larger excitation gap in the Majorana qubit also greatly suppresses the leakage probabilities (see Table I), consistent with the analytic estimates shown in Eq. (7).

IV. QUBIT READOUT

To read out the Majorana qubits, we consider the quantum capacitance measurement as shown in Fig. 4, which is defined as

$$C_q = -\frac{\partial^2 E}{\partial V_g^2}, \tag{9}$$

in the zero-temperature limit [34]. Here, E is the eigenenergy, and V_g is the gate voltage that controls the dot energy via $\mu_{ai} = \alpha_{ai} V_g$, with α_{ai} being the lever arm. Since the measurement is performed when the two chains are decoupled, the result would simply be a sum of the values in each chain, i.e., $C_q = C_{qL} + C_{qR}$. Furthermore, in the equal-lever-arm regime ($\alpha_{a1} = \alpha_{a2} \equiv \alpha$), the quantum capacitance comes only from the even-parity state within each chain, while that of the odd-parity one is strongly suppressed [34]. Thus the quantum capacitances of $|ee\rangle$ and $|oo\rangle$ are

$$C_q^{ee} = \frac{\alpha^2}{\Delta_L} + \frac{\alpha^2}{\Delta_R}, \quad C_q^{oo} = 0, \tag{10}$$

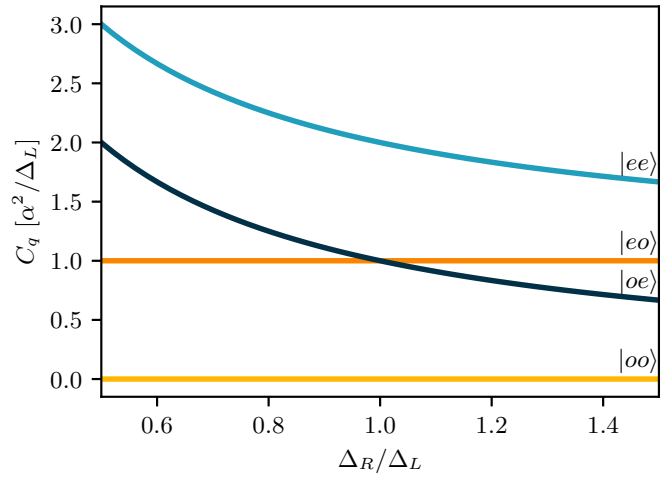

FIG. 4. Quantum capacitance readout in Eq. (9) of the low-energy states in a Majorana qubit. α is the magnitude of the lever arm of the quantum dots, assumed to be identical for all dots. Δ_L (Δ_R) are the superconducting coupling strengths in the left (right) chains.

which are distinct from each other and therefore can be used for qubit readout (see the Appendix G). Following the argument, we further obtain that $C_q^{eo} = \alpha^2/\Delta_L$ and $C_q^{oe} = \alpha^2/\Delta_R$, which are different from both C_q^{ee} and C_q^{oo}. Therefore, in addition to qubit readout, C_q measurement can simultaneously reveal the quasiparticle poisoning effect that transitions a Majorana qubit between states in different total parity space.

V. DISCUSSION

In the numerical simulations, we regard $1/f$ charge noise as the dominant source of decoherence in the proposed devices, neglecting the quasiparticle poisoning effect because this is the prevailing situation in semiconductor platforms. For example, a poisoning time of ∼1 ms, as reported in a similar semiconductor-superconductor hybrid device [59], is much longer than the dephasing time considered here, ∼10 ns, making poisoning insignificant for the current consideration where $1/f$ charge noise dominates decoherence. In addition, here both Rabi and Ramsey experiments are simulated using the most basic protocols for x and z rotations in order to demonstrate the working principles and to provide a fair comparison between semiconductor charge qubits and Majorana qubits. We emphasize that the system we consider [29–32] is equivalent to semiconductor charge qubits if all superconductivity is removed from consideration. It is, therefore, possible to further improve the dephasing time, e.g., by optimizing the pulse profiles, by designing a form of interdot coupling that is more resilient against charge noise, or by further scaling up the Kitaev chain [27,31,60]. Such considerations should be relevant once the basic Rabi and Ramsey oscillations proposed by us are observed so that the elementary concept of a Majorana qubit is established beyond the simplest transport measurements prevalent so far in this subject. We emphasize that our work establishes the feasibility of Rabi oscillations in the already existing experimental platforms of Refs. [29–32].

VI. SUMMARY

We propose and simulate Rabi and Ramsey oscillation experiments for a minimal Majorana qubit defined in coupled quantum dot-superconductor arrays. Our realistic calculations predict actual results of such an experiment and demonstrate that the performance of large-gap Majorana qubits significantly surpasses that of the small-gap counterparts and traditional conventional charge qubits, although some enhancement over semiconductor charge qubits should already manifest in the small-gap platforms. Consequently, conducting such experiments is both feasible and promising on currently available Kitaev chain devices, utilizing existing control and measurement technologies. Our work thus points in an experimental direction of establishing the quantum dot Majorana systems as a viable platform by showing how to perform a completely different experiment, in the context of Majorana systems. This would provide a crucial step toward the realization of the first Majorana qubit in solid-state systems. In fact, the observation of stable Rabi oscillations is synonymous with having a qubit, and our work establishes that such a qubit experiment should be successful in the existing Majorana platforms. The observation of Rabi oscillations in this platform will establish that a feasible qubit exists here, and may also establish that this qubit has substantially enhanced coherence compared with the corresponding semiconductor quantum-dot-based charge qubits with no superconductors.

ACKNOWLEDGMENTS

We are particularly grateful to Xin Zhang, Francesco Zatelli, F. Setiawan, Michael Wimmer, and Jay D. Sau for useful discussions. H.P. is supported by U.S. Office of Naval Research, Grant No. N00014-23-1-2357. C.-X.L. is supported by a subsidy for top consortia for knowledge and innovation (TKI subsidiary). S.D.S. is supported by the Laboratory for Physical Sciences through the Condensed Matter Theory Center at the University of Maryland.

APPENDIX A: MODEL

The system of the double two-site Kitaev chain is described by the following Hamiltonian:

$$\mathcal{H} = \mathcal{H}_L + \mathcal{H}_R + \mathcal{H}_T + \mathcal{H}_\mu, \tag{A1}$$

where intrachain coupling in the left chain (site index 1 and 2) and right chain (site index 3 and 4) is

$$\mathcal{H}_L = t\sum(c_{L2}^\dagger c_{L1} + c_{L1}^\dagger c_{L2}) + \Delta(c_{L2}c_{L1} + c_{L1}^\dagger c_{L2}^\dagger),$$

$$\mathcal{H}_R = t\sum(c_{R2}^\dagger c_{R1} + c_{R1}^\dagger c_{R2}) + \Delta(c_{R2}c_{R1} + c_{R1}^\dagger c_{R2}^\dagger), \tag{A2}$$

the interchain hopping is

$$\mathcal{H}_T = \Gamma(c_{R1}^\dagger c_{L2} + c_{L2}^\dagger c_{R1}), \tag{A3}$$

and the on-site chemical potential is

$$\mathcal{H}_\mu = \sum_{a\in\{L,R\}}\sum_{i=1}^{2}\mu_i c_{a,i}^\dagger c_{a,i}. \tag{A4}$$

Up to a particle-hole transformation, we can choose $t > 0$, $\Delta > 0$, and $\Gamma > 0$.

Here, without the tunneling term $\Gamma = 0$, the two chains are decoupled, where the sweet spot is achieved when $t = \Delta$, and $\mu_i = 0$, leading to the ground-state manifold spanned by

$$|e\rangle_L = \frac{1}{\sqrt{2}}(1 - c_{L1}^\dagger c_{L2}^\dagger)|0\rangle, \quad |o\rangle_L = \frac{1}{\sqrt{2}}(c_{L1}^\dagger - c_{L2}^\dagger)|0\rangle, \tag{A5}$$

$$|e\rangle_R = \frac{1}{\sqrt{2}}(1 - c_{R1}^\dagger c_{R2}^\dagger)|0\rangle, \quad |o\rangle_R = \frac{1}{\sqrt{2}}(c_{R1}^\dagger - c_{R2}^\dagger)|0\rangle, \tag{A6}$$

for the left and right systems, respectively.

With the tunneling term, the ground state of the two chains can be spanned by the two other single-chain excited states denoted as

$$|e'\rangle_L = \frac{1}{\sqrt{2}}(1 + c_{L1}^\dagger c_{L2}^\dagger)|0\rangle, \quad |o'\rangle_L = \frac{1}{\sqrt{2}}(c_{L1}^\dagger + c_{L2}^\dagger)|0\rangle, \tag{A7}$$

$$|e'\rangle_R = \frac{1}{\sqrt{2}}(1 + c_{R1}^\dagger c_{R2}^\dagger)|0\rangle, \quad |o'\rangle_R = \frac{1}{\sqrt{2}}(c_{R1}^\dagger + c_{R2}^\dagger)|0\rangle. \tag{A8}$$

Therefore, $|e\rangle_L$, $|e'\rangle_L$, $|o\rangle_L$, and $|o'\rangle_L$ ($|e\rangle_R$, $|e'\rangle_R$, $|o\rangle_R$, and $|o'\rangle_R$) form the complete basis for the left (right) chain.

Without the loss of generality, we choose to work in the even total parity, leading to a complete basis of $|ee\rangle \equiv |e\rangle_L|e\rangle_R$, $|oo\rangle$, $|e'e'\rangle$, $|o'o'\rangle$, $|ee'\rangle$, $|oo'\rangle$, $|e'e\rangle$, and $|o'o\rangle$. With this set of bases, the matrix representation of the sum of Hamiltonian (A2) and (A3) is

$$H_L + H_R + H_T = \begin{pmatrix} h_+ & 0 \\ 0 & h_- \end{pmatrix}, \tag{A9}$$

where h_+ and h_- are

$$h_+ = \begin{pmatrix} -2\Delta & -\Gamma/2 & 0 & -\Gamma/2 \\ -\Gamma/2 & -2t & \Gamma/2 & 0 \\ 0 & \Gamma/2 & 2\Delta & \Gamma/2 \\ -\Gamma/2 & 0 & \Gamma/2 & 2t \end{pmatrix}, \tag{A10}$$

$$h_- = \begin{pmatrix} 0 & \Gamma/2 & 0 & \Gamma/2 \\ \Gamma/2 & 0 & -\Gamma/2 & 0 \\ 0 & -\Gamma/2 & 0 & -\Gamma/2 \\ \Gamma/2 & 0 & -\Gamma/2 & 0 \end{pmatrix}. \tag{A11}$$

Similarly, the matrix representation of the on-site chemical potential given by Eq. (A4) is

$$H_\mu = \frac{\mu_{1234}}{2}\mathbb{1} + \frac{1}{2}\begin{pmatrix} 0 & h_\mu \\ h_\mu^\dagger & 0 \end{pmatrix}, \tag{A12}$$

where

$$h_\mu = \begin{pmatrix} -\mu_{34} & 0 & -\mu_{12} & 0 \\ 0 & \delta\mu_{34} & 0 & \delta\mu_{12} \\ -\mu_{12} & 0 & -\mu_{34} & 0 \\ 0 & \delta\mu_{12} & 0 & \delta\mu_{34} \end{pmatrix}, \tag{A13}$$

with the shorthand notions of $\mu_{1234} \equiv \sum_{i=1}^{4} \mu_i$, $\mu_{12} \equiv \mu_1 + \mu_2$, $\mu_{34} \equiv \mu_3 + \mu_4$, $\delta\mu_{12} \equiv \mu_1 - \mu_2$, and $\delta\mu_{34} \equiv \mu_3 - \mu_4$.

APPENDIX B: LEAKAGE DUE TO Δ, t, AND Γ

In Eq. (3) in the main text, we considered the disorder effect in ϵ and Γ before σ_z and σ_x. Here, we will consider their leakage effect separately to understand the leakage that is effectively on ϵ and Γ.

We first consider the effect of the disorder only in Δ, t, and Γ, i.e., $\mu_i = 0$, because Eq. (A9) is block diagonal, and given the initial state is $|ee\rangle$, we only need to consider the subspace of h_+, where the Rabi oscillation is between $|ee\rangle$ and $|oo\rangle$ and the leakage states are $|e'e'\rangle$ and $|o'o'\rangle$.

We use the time-dependent perturbation theory, where Eq. (A9) is decomposed into the noninteracting part H_0,

$$H_0 = \begin{pmatrix} -2\Delta & -\Gamma/2 & 0 & 0 \\ -\Gamma/2 & -2t & 0 & 0 \\ 0 & 0 & 2\Delta & \Gamma/2 \\ 0 & 0 & \Gamma/2 & 2t \end{pmatrix}, \tag{B1}$$

and the perturbation H_1 as

$$H_1 = \begin{pmatrix} 0 & 0 & 0 & -\Gamma/2 \\ 0 & 0 & \Gamma/2 & 0 \\ 0 & \Gamma/2 & 0 & 0 \\ -\Gamma/2 & 0 & 0 & 0 \end{pmatrix}. \tag{B2}$$

Conceptually, the first term H_0 in Eq. (B1) accounts for the Rabi oscillation between $|ee\rangle$ and $|oo\rangle$ (given the initial state is $|ee\rangle$), and the second term H_1 in Eq. (B2) leads to $|e'e'\rangle$ and $|o'o'\rangle$.

The time-evolution operator (in the Schrödinger picture) is expanded in the Dyson series (truncated at the first order) as

$$U(\tau) = e^{-iH_0\tau}\left[1 - i\int_0^\tau d\tau_1 H_{1,I}(\tau_1)\right]e^{iH_0\tau}, \tag{B3}$$

where $H_{1,I}(\tau_1)$ is H_1 in the interacting picture,

$$H_{1,I}(\tau_1) = e^{iH_0\tau}H_1 e^{-iH_0\tau} = \sum_{i,j}\langle i|H_1|j\rangle e^{i(E_i-E_j)\tau_1}, \tag{B4}$$

and $|i\rangle$ is the eigenvector of H_0 with the eigenvalues of E_i.

The spectrum of H_0 in Eq. (B1) is

$$\begin{aligned} -E_+ &: \quad \left(\cos\left(\tfrac{\theta}{2}\right) \quad \sin\left(\tfrac{\theta}{2}\right) \quad 0 \quad 0\right)^\intercal, \\ -E_- &: \quad \left(-\sin\left(\tfrac{\theta}{2}\right) \quad \cos\left(\tfrac{\theta}{2}\right) \quad 0 \quad 0\right)^\intercal, \\ E_- &: \quad \left(0 \quad 0 \quad -\sin\left(\tfrac{\theta}{2}\right) \quad \cos\left(\tfrac{\theta}{2}\right)\right)^\intercal, \\ E_+ &: \quad \left(0 \quad 0 \quad \cos\left(\tfrac{\theta}{2}\right) \quad \sin\left(\tfrac{\theta}{2}\right)\right)^\intercal, \end{aligned} \tag{B5}$$

where $E_\pm = \Delta + t \pm \sqrt{(\Delta - t)^2 + (\Gamma/2)^2}$ and $\tan\theta = \frac{\Gamma/2}{\Delta - t}$. We substitute the eigenvectors and eigenvalues of H_0 into Eq. (B4), with the initial state

$$|\psi(\tau = 0)\rangle = |ee\rangle = (1 \quad 0 \quad 0 \quad 0)^\intercal, \tag{B6}$$

and we have the (unnormalized) final state in the Schrödinger picture as

$$\begin{aligned} |\psi(\tau)\rangle &= U(\tau)|\psi(\tau = 0)\rangle = |\psi(\tau)\rangle \\ &= \begin{pmatrix} e^{i\omega\tau}[\cos(\Omega\tau) + i\sin(\Omega\tau)\cos\theta] \\ e^{i\omega\tau} i\sin(\Omega\tau)\sin\theta \\ \frac{\Gamma}{2\omega}\sin(\omega\tau)\sin(\Omega\tau)\sin\theta \\ \frac{\Gamma}{2\omega}[-\sin(\Omega\tau)\cos\theta + i\cos(\Omega\tau)]\sin(\omega\tau) \end{pmatrix}, \end{aligned} \tag{B7}$$

where $\Omega = \sqrt{(\Delta - t)^2 + (\Gamma/2)^2}$ and $\omega = \Delta + t$.

Therefore, the Rabi oscillations between $|ee\rangle$ and $|oo\rangle$ have the probability densities of

$$\begin{aligned} P_{ee}(\tau) &= |\langle ee|\psi(\tau)\rangle|^2 = \sin^2(\Omega\tau)\cos^2(\theta) + \cos^2(\Omega\tau), \\ P_{oo}(\tau) &= |\langle oo|\psi(\tau)\rangle|^2 = \sin^2(\theta)\sin^2(\Omega\tau), \end{aligned} \tag{B8}$$

and the leakage is

$$\begin{aligned} P_{\text{leak}}(\tau) &= P_{e'e'}(\tau) + P_{o'o'}(\tau) = |\langle e'e'|\psi(\tau)\rangle|^2 + |\langle o'o'|\psi(\tau)\rangle|^2 \\ &= \frac{\Gamma^2\sin^2(\omega\tau)}{4\omega^2}, \end{aligned} \tag{B9}$$

indicating that the leakage frequency is $2\omega = 2(\Delta + t)$, which is independent of the Γ and consistent with Fig. 2(b) in the main text.

Specifically, at the sweep spot $\Delta = t$, we have $\theta = \pi/2$ and the probability densities are

$$\begin{aligned} P_{ee}(\tau) &= \cos^2(\Omega\tau), \\ P_{oo}(\tau) &= \sin^2(\Omega\tau), \\ P_{\text{leak}}(\tau) &= \frac{\Gamma^2}{16\Delta^2}\sin^2(2\Delta\tau), \end{aligned} \tag{B10}$$

recovering the Rabi frequency $2\Omega = \Gamma$ in Fig. 2(a).

APPENDIX C: LEAKAGE DUE TO μ_1

To consider the leakage effect in μ_1 (or, equivalently, for μ_4 due to the inversion symmetry), we set all other parameters to the sweet spot, including $\Delta = t_0$ and $\mu_2 = \mu_3 = \mu_4 = 0$. Following the same time-dependent perturbation theory, the noninteracting part $H_0^{\mu_1}$ is

$$H_0^{\mu_1} = \frac{\mu_1}{2}\mathbb{1} + \begin{pmatrix} H_0 & 0 \\ 0 & h_- \end{pmatrix}, \tag{C1}$$

where H_0 and h_- are in Eq. (B1) and in Eq. (A11) (with $\Delta = t$), and the perturbation term $H_1^{\mu_1}$ is

$$H_1^{\mu_1} = \begin{pmatrix} H_1 & h_{\mu_1} \\ h_{\mu_1}^\dagger & 0 \end{pmatrix}, \tag{C2}$$

where H_1 is in Eq. (B2) and H_{μ_1} is

$$h_{\mu_1} = \frac{1}{2}\begin{pmatrix} 0 & 0 & -\mu_1 & 0 \\ 0 & 0 & 0 & \mu_1 \\ -\mu_1 & 0 & 0 & 0 \\ 0 & \mu_1 & 0 & 0 \end{pmatrix}, \tag{C3}$$

from Eq. (A13).

Here, the noninteracting term $H_0^{\mu_1}$ has the eigenvalues and eigenvectors as

$$\begin{aligned}
-2\Delta-\frac{\Gamma}{2}+\frac{\mu_1}{2}:&\quad \frac{1}{\sqrt{2}}(1\quad 1\quad 0\quad 0\quad 0\quad 0\quad 0\quad 0)^{\mathsf{T}},\\
-2\Delta+\frac{\Gamma}{2}+\frac{\mu_1}{2}:&\quad \frac{1}{\sqrt{2}}(-1\quad 1\quad 0\quad 0\quad 0\quad 0\quad 0\quad 0)^{\mathsf{T}},\\
2\Delta-\frac{\Gamma}{2}+\frac{\mu_1}{2}:&\quad \frac{1}{\sqrt{2}}(0\quad 0\quad -1\quad 1\quad 0\quad 0\quad 0\quad 0)^{\mathsf{T}},\\
2\Delta+\frac{\Gamma}{2}+\frac{\mu_1}{2}:&\quad \frac{1}{\sqrt{2}}(0\quad 0\quad 1\quad 1\quad 0\quad 0\quad 0\quad 0)^{\mathsf{T}},\\
\frac{\mu_1}{2}:&\quad \frac{1}{\sqrt{2}}(0\quad 0\quad 0\quad 0\quad 1\quad 0\quad 1\quad 0)^{\mathsf{T}},\\
\frac{\mu_1}{2}:&\quad \frac{1}{\sqrt{2}}(0\quad 0\quad 0\quad 0\quad 0\quad -1\quad 0\quad 1)^{\mathsf{T}},\\
-\Gamma+\frac{\mu_1}{2}:&\quad \frac{1}{2}(0\quad 0\quad 0\quad 0\quad 1\quad 1\quad -1\quad 1)^{\mathsf{T}},\\
\Gamma+\frac{\mu_1}{2}:&\quad \frac{1}{2}(0\quad 0\quad 0\quad 0\quad -1\quad 1\quad 1\quad 1)^{\mathsf{T}}.
\end{aligned}\tag{C4}$$

With the initial state $|ee\rangle=(1\quad 0\quad 0\quad 0\quad 0\quad 0\quad 0\quad 0)^{\mathsf{T}}$, the (unnormalized) final state in the Schrödinger picture is

$$\psi^{\mu_1}(\tau)=\begin{pmatrix}
e^{i\tau(2\Delta-\frac{\mu_1}{2})}\cos\left(\frac{\tau\Gamma}{2}\right)\\
ie^{i\tau(2\Delta-\frac{\mu_1}{2})}\sin\left(\frac{\tau\Gamma}{2}\right)\\
\frac{\Gamma}{4\Delta}e^{-\frac{i\tau\mu_1}{2}}\sin(2\tau\Delta)\sin\left(\frac{\tau\Gamma}{2}\right)\\
\frac{i\Gamma}{4\Delta}e^{-\frac{i\tau\mu_1}{2}}\sin(2\tau\Delta)\cos\left(\frac{\tau\Gamma}{2}\right)\\
\frac{1}{2}\mu_1 e^{i\tau(\Delta-\frac{\mu_1}{2})}\sin\left(\frac{\tau\Gamma}{2}\right)\left[\frac{1}{E_-}e^{\frac{i\tau\Gamma}{4}}\sin\left(\frac{E_-\tau}{2}\right)-\frac{1}{E_+}e^{-\frac{i\tau\Gamma}{4}}\sin\left(\frac{E_+\tau}{2}\right)\right]\\
\frac{1}{2}\mu_1 e^{i\tau(\Delta-\frac{\mu_1}{2})}\cos\left(\frac{\tau\Gamma}{2}\right)\left[-\frac{1}{E_-}ie^{\frac{i\tau\Gamma}{4}}\sin\left(\frac{E_-\tau}{2}\right)+\frac{1}{E_+}ie^{-\frac{i\tau\Gamma}{4}}\sin\left(\frac{E_+\tau}{2}\right)\right]\\
\frac{1}{2}\mu_1 e^{i\tau(\Delta-\frac{\mu_1}{2})}\cos\left(\frac{\tau\Gamma}{2}\right)\left[\frac{1}{E_-}ie^{\frac{i\tau\Gamma}{4}}\sin\left(\frac{E_-\tau}{2}\right)+\frac{1}{E_+}ie^{-\frac{i\tau\Gamma}{4}}\sin\left(\frac{E_+\tau}{2}\right)\right]\\
\frac{1}{2}\mu_1 e^{i\tau(\Delta-\frac{\mu_1}{2})}\sin\left(\frac{\tau\Gamma}{2}\right)\left[\frac{1}{E_-}e^{\frac{i\tau\Gamma}{4}}\sin\left(\frac{E_-\tau}{2}\right)+\frac{1}{E_+}e^{-\frac{i\tau\Gamma}{4}}\sin\left(\frac{E_+\tau}{2}\right)\right]
\end{pmatrix},\tag{C5}$$

where $E_\pm=2\Delta\pm\Gamma/2$.

Therefore, the leakage to the $|e'e'\rangle$ and $|o'o'\rangle$ is the same,

$$P_{e'e'}(\tau)+P_{o'o'}(\tau)=|\langle e'e'|\psi^{\mu_1}(\tau)\rangle|^2+|\langle o'o'|\psi^{\mu_1}(\tau)\rangle|^2=\frac{\Gamma^2\sin^2(2\tau\Delta)}{16\Delta^2},\tag{C6}$$

and the leakage to $|ee'\rangle$, $|oo'\rangle$, $|e'e\rangle$, and $|o'o\rangle$ is

$$\begin{aligned}
P_{ee'}(\tau)+P_{oo'}(\tau)+P_{e'e}(\tau)+P_{o'o}(\tau)&=|\langle ee'|\psi^{\mu_1}(\tau)\rangle|^2+|\langle oo'|\psi^{\mu_1}(\tau)\rangle|^2+|\langle e'e|\psi^{\mu_1}(\tau)\rangle|^2+|\langle o'o|\psi^{\mu_1}(\tau)\rangle|^2\\
&=\frac{\mu_1^2}{2}\left(\frac{\sin^2\left(\frac{E_-\tau}{2}\right)}{E_-^2}+\frac{\sin^2\left(\frac{E_+\tau}{2}\right)}{E_+^2}\right).
\end{aligned}\tag{C7}$$

This introduces a superposition of two frequencies E_- and E_+ in the leakage frequency, where the envelope frequency is $E_-+E_+=4\Delta$ and the carrier frequency is $E_+-E_-=\Gamma$.

APPENDIX D: LEAKAGE DUE TO μ_2

The leakage effect in the other on-site chemical potential is μ_2 (or μ_3). Namely, we set $\mu_1=\mu_3=\mu_4=0$, and $t=\Delta$. This leads to the same noninteracting part $H_0^{\mu_2}=H_0^{\mu_1}$ as in Eq. (C1), while the perturbation term $H_1^{\mu_2}$ is

$$H_1^{\mu_2}=\begin{pmatrix}H_1 & h_{\mu_2}\\ h_{\mu_2}^\dagger & 0\end{pmatrix},\tag{D1}$$

where H_1 is in Eq. (B2) and h_{μ_2} is

$$h_{\mu_2} = \frac{1}{2}\begin{pmatrix} 0 & 0 & -\mu_2 & 0 \\ 0 & 0 & 0 & -\mu_2 \\ -\mu_2 & 0 & 0 & 0 \\ 0 & -\mu_2 & 0 & 0 \end{pmatrix}. \tag{D2}$$

Here, the noninteracting term $H_0^{\mu_2}$ has the same eigenvalues (with μ_1 replaced with μ_2) and eigenvectors as in Eq. (C4), and, therefore, the final state in the Schrödinger picture starting from $|ee\rangle$ is

$$\psi^{\mu_2}(\tau) = \begin{pmatrix} e^{i\tau(2\Delta-\frac{\mu_2}{2})}\cos\left(\frac{\tau\Gamma}{2}\right) \\ ie^{i\tau(2\Delta-\frac{\mu_2}{2})}\sin\left(\frac{\tau\Gamma}{2}\right) \\ \frac{\Gamma}{4\Delta}e^{-\frac{i\tau\mu_2}{2}}\sin(2\tau\Delta)\sin\left(\frac{\tau\Gamma}{2}\right) \\ \frac{i\Gamma}{4\Delta}e^{-\frac{i\tau\mu_2}{2}}\sin(2\tau\Delta)\cos\left(\frac{\tau\Gamma}{2}\right) \\ \frac{\mu_2}{4}e^{i\tau(\Delta-\frac{\mu_2}{2})}\left[\left(\frac{i\sin\left(\frac{E_-\tau}{2}\right)}{E_-}-\frac{i\sin\left(\frac{E'_+\tau}{2}\right)}{E'_+}\right)e^{-\frac{i\tau\Gamma}{4}}+\left(-\frac{i\sin\left(\frac{E'_-\tau}{2}\right)}{E'_-}+\frac{i\sin\left(\frac{E_+\tau}{2}\right)}{E_+}\right)e^{\frac{i\tau\Gamma}{4}}\right] \\ \frac{\mu_2}{4}e^{i\tau(\Delta-\frac{\mu_2}{2})}\left[\left(\frac{i\sin\left(\frac{E_-\tau}{2}\right)}{E_-}+\frac{i\sin\left(\frac{E'_+\tau}{2}\right)}{E'_+}\right)e^{-\frac{i\tau\Gamma}{4}}+\left(-\frac{i\sin\left(\frac{E'_-\tau}{2}\right)}{E'_-}-\frac{i\sin\left(\frac{E_+\tau}{2}\right)}{E_+}\right)e^{\frac{i\tau\Gamma}{4}}\right] \\ \frac{\mu_2}{4}e^{i\tau(\Delta-\frac{\mu_2}{2})}\left[\left(\frac{i\sin\left(\frac{E_-\tau}{2}\right)}{E_-}+\frac{i\sin\left(\frac{E'_+\tau}{2}\right)}{E'_+}\right)e^{-\frac{i\tau\Gamma}{4}}+\left(\frac{i\sin\left(\frac{E'_-\tau}{2}\right)}{E'_-}+\frac{i\sin\left(\frac{E_+\tau}{2}\right)}{E_+}\right)e^{\frac{i\tau\Gamma}{4}}\right] \\ \frac{\mu_2}{4}e^{i\tau(\Delta-\frac{\mu_2}{2})}\left[\left(-\frac{i\sin\left(\frac{E_-\tau}{2}\right)}{E_-}+\frac{i\sin\left(\frac{E'_+\tau}{2}\right)}{E'_+}\right)e^{-\frac{i\tau\Gamma}{4}}+\left(-\frac{i\sin\left(\frac{E'_-\tau}{2}\right)}{E'_-}+\frac{i\sin\left(\frac{E_+\tau}{2}\right)}{E_+}\right)e^{\frac{i\tau\Gamma}{4}}\right] \end{pmatrix}, \tag{D3}$$

where $E_\pm = 2\Delta \pm \Gamma/2$ and $E'_\pm = 2\Delta \pm 3\Gamma/2$.

Therefore, the leakage to the $|e'e'\rangle$ and $|o'o'\rangle$ is the same as Eq. (C7), and the leakage to $|ee'\rangle$, $|oo'\rangle$, $|e'e\rangle$, and $|o'o\rangle$ is

$$\begin{aligned} P_{ee'}(\tau)+P_{oo'}(\tau)+P_{e'e}(\tau)+P_{o'o}(\tau) &= |\langle ee'|\psi^{\mu_2}(\tau)\rangle|^2+|\langle oo'|\psi^{\mu_2}(\tau)\rangle|^2+|\langle e'e|\psi^{\mu_2}(\tau)\rangle|^2+|\langle o'o|\psi^{\mu_2}(\tau)\rangle|^2 \\ &= \frac{\mu_2^2}{4}\left(\frac{\sin^2\left(\frac{E_-\tau}{2}\right)}{E_-^2}+\frac{\sin^2\left(\frac{E_+\tau}{2}\right)}{E_+^2}+\frac{\sin^2\left(\frac{E'_-\tau}{2}\right)}{{E'_-}^2}+\frac{\sin^2\left(\frac{E'_+\tau}{2}\right)}{{E'_+}^2}\right). \end{aligned} \tag{D4}$$

APPENDIX E: DEPHASING DUE TO DISORDER IN Γ

In this Appendix, we consider the dephasing effect which is used to estimate T_2. To focus only on the low-energy sector, we work in the minimal two-level system where the Hilbert space only includes $|ee\rangle$ and $|oo\rangle$. The effect of Γ acts like the magnetic field along the x direction and, therefore, the effective two-level Hamiltonian is

$$H_x = B_x\sigma_x, \tag{E1}$$

where B_x is quasistatic disorder following the Gaussian distribution with the variance of $\sigma_{B_x}^2$ and mean of $\bar{B}_x$, i.e., $B_x \sim \mathcal{N}(\bar{B}_x, \sigma_{B_x}^2)$, σ_x is the Pauli X matrix, and the initial state is $\psi_x(\tau=0) = |ee\rangle$.

Under the evolution of H_x, the final state $\psi_x(\tau)$ is

$$\psi_x(\tau) = e^{-iH_x\tau}\psi_x(\tau=0) = \begin{pmatrix} \cos(B_x\tau) \\ -i\sin(B_x\tau) \end{pmatrix}. \tag{E2}$$

Therefore, the probability of finding the state in $|oo\rangle$ is

$$P_{oo}(\tau) = |\langle oo|\psi_x(\tau)\rangle|^2 = \sin^2(B_x\tau). \tag{E3}$$

Thus, the disorder-averaged probability is

$$\begin{aligned} \langle P_{oo}(\tau)\rangle_{B_x} &= \frac{1}{\sqrt{2\pi}\sigma_{B_x}}\int_{-\infty}^{\infty} dB_x e^{-\frac{(B_x-\bar{B}_x)^2}{2\sigma_{B_x}^2}}\sin^2(B_x\tau) \\ &= \frac{1}{2}[1+e^{-2\tau^2\sigma_{B_x}^2}\cos(2\bar{B}_x\tau)]. \end{aligned} \tag{E4}$$

Therefore, the decay of the envelope of $\langle P_{oo}(\tau)\rangle_{B_x}$ follows the Gaussian decay with a prefactor of $e^{-2\tau^2\sigma_{B_x}^2}$, namely, $\beta = 2$ in the ansatz in Eq. (5) in the main text. This provides a fundamental understanding of the ansatz in Eq. (5) in the main text.

APPENDIX F: DEPHASING DUE TO DISORDER IN μ_i, Δ, AND t

Besides the dephasing effect due to the disorder in Γ, we also consider the dephasing effect due to the disorder in μ_i, Δ, and t.

In practice, the disorder of these quantities acts like the magnetic field along the z direction and, therefore, the effective two-level Hamiltonian is

$$H_{xz} = B_x\sigma_x + B_z\sigma_z, \tag{F1}$$

where B_x here is constant, B_z is quasistatic disorder following the Gaussian distribution with the variance of $\sigma_{B_z}^2$ and mean of 0, i.e., $B_z \sim \mathcal{N}(0, \sigma_{B_z}^2)$, σ_z is the Pauli Z matrix, and the initial state is again $\psi_{xz}(\tau = 0) = |ee\rangle$.

Under the evolution of H_{xz}, the final state $\psi_{xz}(\tau)$ is

$$\psi_{xz}(\tau) = e^{-iH_{xz}\tau}\psi_{xz}(\tau = 0) = \begin{pmatrix} \cos\left(\sqrt{B_x^2 + B_z^2}\tau\right) - i\sin\left(\sqrt{B_x^2 + B_z^2}\tau\right)\cos(\theta) \\ -i\sin\left(\sqrt{B_x^2 + B_z^2}\tau\right)\sin(\theta) \end{pmatrix}, \tag{F2}$$

where $\tan\theta = B_x/B_z$, and the probability of finding the state in $|oo\rangle$ is

$$P_{oo}(\tau) = |\langle oo|\psi_{xz}(\tau)\rangle|^2 = \sin^2\left(\sqrt{B_x^2 + B_z^2}\tau\right)\frac{B_x^2}{B_x^2 + B_z^2}. \tag{F3}$$

Therefore, the disorder-averaged probability is

$$\begin{aligned} &\langle P_{oo}(\tau)\rangle_{B_z} \\ &= \frac{1}{\sqrt{2\pi}\sigma_{B_z}}\int_{-\infty}^{\infty} dB_z e^{-\frac{B_z^2}{2\sigma_{B_z}^2}} \sin^2\left(\sqrt{B_x^2 + B_z^2}\tau\right)\frac{B_x^2}{B_x^2 + B_z^2} \\ &\approx \frac{1}{\sqrt{2\pi}\sigma_{B_z}}\int_{-\infty}^{\infty} dB_z e^{-\frac{B_z^2}{2\sigma_{B_z}^2}} \sin^2\left[\left(B_x^2 + \frac{B_z^2}{2B_x}\right)\tau\right] \\ &= \frac{1}{4}\left(2 - \frac{B_x e^{2iB_x\tau}}{\sqrt{B_x\left(B_x - 2i\sigma_{B_z}^2\tau\right)}} - \frac{B_x e^{-2iB_x\tau}}{\sqrt{B_x\left(B_x + 2i\sigma_{B_z}^2\tau\right)}}\right), \end{aligned} \tag{F4}$$

where the second line assumes the $B_z \ll B_x$ such that $\sqrt{B_x^2 + B_z^2} \approx B_x + \frac{B_z^2}{2B_x}$, and $\frac{B_x^2}{B_x^2 + B_z^2} \approx 1$. Therefore, it shows a power-law decay with $\langle P_{oo}(\tau)\rangle_{B_z} \sim \tau^{-\frac{1}{2}}$.

We provide the parameter for the numerical simulations of qubit dephasing in Figs. 3(d)–3(f). For the charge qubit in Fig. 3(d), we set $\varepsilon_{L/R} \sim \mathcal{N}(0, 3^2)$, $\Gamma_{L/R} \sim \mathcal{N}(5, 0.05^2)$ during the x pulse (i.e., with finite $\Gamma_{L/R}$) in units of meV, where $\mathcal{N}(\mu, \sigma^2)$ is the normal distribution with mean μ and variance σ^2; during the z pulse (i.e., with finite $\varepsilon_{L/R}$), we set $\varepsilon_L \sim \mathcal{N}(20, 3^2)$, $\varepsilon_R \sim \mathcal{N}(-20, 3^2)$, $\Gamma_{L/R} \sim \mathcal{N}(0, 0.05^2)$ in units of meV. For the small-gap Majorana qubit (all four $\Delta_{1,2,3,4} = 12$ meV) as shown in Fig. 3(e), during the x pulse, we set four $\mu_{1,2,3,4} \sim \mathcal{N}(0, 3^2)$, $t_{L/R} \sim \mathcal{N}(12, 0.016^2)$, and $\Gamma = 0.5$ meV; during the z pulse, we set four $\mu_{1,2,3,4} \sim \mathcal{N}(0, 3^2)$, $t_L \sim \mathcal{N}(14, 0.016^2)$, $t_R \sim \mathcal{N}(12, 0.016^2)$, and $\Gamma = 0$ meV. For the large-gap Majorana qubit (all four $\Delta_{1,2,3,4} = 38$ meV) as shown in Fig. 3(f), during the x pulse, we set four $\mu_{1,2,3,4} \sim \mathcal{N}(0, 0.3^2)$, $t_{L/R} \sim \mathcal{N}(38, 0.016^2)$, and $\Gamma = 0.5$ meV; during the z pulse, we set four $\mu_{1,2,3,4} \sim \mathcal{N}(0, 0.3^2)$, $t_L \sim \mathcal{N}(40, 0.016^2)$, $t_R \sim \mathcal{N}(38, 0.016^2)$, and $\Gamma = 0$ meV.

APPENDIX G: QUANTUM CAPACITANCE MEASUREMENT OF A MAJORANA QUBIT

In this Appendix, we show that the quantum capacitance measurement is capable of reading out $|ee\rangle$ and $|oo\rangle$ in a Majorana qubit. We first review the calculations in a single Kitaev chain, and then generalize it to a Majorana qubit composed of double Kitaev chains. The zero-temperature quantum capacitance of a state is defined as

$$C_q = -\frac{\partial^2 E}{\partial V_g^2}, \tag{G1}$$

where E is the eigenenergy of the state and V_g is the gate voltage. The Hamiltonian of a minimal Kitaev chain can be decomposed into even- and odd-parity sectors due to Fermi parity conservation. The even-parity Hamiltonian is

$$H_{\text{even}} = \begin{pmatrix} |00\rangle \\ |11\rangle \end{pmatrix}^T \begin{pmatrix} 0 & \Delta \\ \Delta & \mu_1 + \mu_2 \end{pmatrix}\begin{pmatrix} \langle 00| \\ \langle 11| \end{pmatrix}, \tag{G2}$$

where $\mu_{1,2}$ are the on-site energies of the two dots and t, Δ are the normal and Andreev couplings. The ground-state energy E_e of $|e\rangle$ is

$$E_e = \frac{\mu_1 + \mu_2}{2} - \sqrt{\Delta^2 + \left(\frac{\mu_1 + \mu_2}{2}\right)^2}. \tag{G3}$$

On the other hand, the derivative with respect to gate voltage is

$$\frac{\partial}{\partial V_g} = \alpha_1\frac{\partial}{\partial \mu_1} + \alpha_2\frac{\partial}{\partial \mu_2} \approx \alpha\left(\frac{\partial}{\partial \mu_1} + \frac{\partial}{\partial \mu_2}\right), \tag{G4}$$

where $\alpha_i \equiv d\mu_i/dV_g$ is the lever arm, and here we assume that all dots share a similar value of lever arm α. Therefore, it is straightforward to obtain the quantum capacitance of the even-parity ground state as below,

$$C_q^e = -\frac{\partial^2 E_e}{\partial V_g^2} = \frac{\alpha^2}{\sqrt{\Delta^2 + \left(\frac{\mu_1+\mu_2}{2}\right)^2}} - \frac{\alpha^2(\mu_1 + \mu_2)^2}{4\left[\Delta^2 + \left(\frac{\mu_1+\mu_2}{2}\right)^2\right]^{3/2}}. \tag{G5}$$

At the sweet spot of $\mu_1 = \mu_2 = 0$, we have

$$C_q^e = \frac{\alpha^2}{\Delta}. \tag{G6}$$

On the other hand, the Hamiltonian in the odd-parity sector is

$$H_{\text{odd}} = \begin{pmatrix} |10\rangle \\ |01\rangle \end{pmatrix}^T \begin{pmatrix} \mu_1 & t \\ t & \mu_2 \end{pmatrix}\begin{pmatrix} \langle 10| \\ \langle 01| \end{pmatrix}, \tag{G7}$$

with the ground-state energy being

$$E_o = \frac{\mu_1 + \mu_2}{2} - \sqrt{t^2 + \left(\frac{\mu_1 - \mu_2}{2}\right)^2}. \tag{G8}$$

The corresponding quantum capacitance is

$$C_q^o = 0, \tag{G9}$$

due to the opposite signs of the coefficients in front of μ_1 and μ_2 in the term of $(\frac{\mu_1-\mu_2}{2})^2$.

We now generalize our calculations to the quantum capacitance of the double Kitaev chain system. The eigenenergies

of the ground states are simply the sum of the left and right chains, i.e.,

$$E_{ab} = E_{aL}(\mu_{L1}, \mu_{L2}) + E_{bR}(\mu_{R1}, \mu_{R2}), \tag{G10}$$

where a, b denotes the parity e, o. We note that the μ dependence of E is separable between the left and right chains, which indicates that $\partial/\partial V_g \to \alpha(\frac{\partial}{\partial \mu_{L1}} + \frac{\partial}{\partial \mu_{L2}})$ for the left chain energy, while $\partial/\partial V_g \to \alpha(\frac{\partial}{\partial \mu_{R1}} + \frac{\partial}{\partial \mu_{R2}})$ for the right one. Therefore, we have

$$C_q^{ab} = -\frac{\partial^2 E_{ab}}{\partial V_g^2} = -\frac{\partial^2 E_{aL}}{\partial V_g^2} - \frac{\partial^2 E_{bR}}{\partial V_g^2} = C_q^{aL} + C_q^{bR}, \tag{G11}$$

that is, the quantum capacitance of the state in the whole system is a sum of the value in each chain separately. We therefore have

$$\begin{aligned} C_q^{ee} &= \frac{\alpha^2}{\Delta_L} + \frac{\alpha^2}{\Delta_R}, \\ C_q^{oo} &= 0, \\ C_q^{eo} &= \frac{\alpha^2}{\Delta_L}, \\ C_q^{oe} &= \frac{\alpha^2}{\Delta_R}. \end{aligned} \tag{G12}$$

Therefore, one can distinguish between $|ee\rangle$ and $|oo\rangle$ states using the quantum capacitance measurement. Furthermore, the values of C_q for $|eo\rangle$ and $|oe\rangle$ are generally very different from the qubit states. Thus our method also provides a possible way to investigate the quasiparticle poisoning effect by analyzing the readout results of $|eo\rangle$ and $|oe\rangle$.

[1] N. Read and D. Green, Paired states of fermions in two dimensions with breaking of parity and time-reversal symmetries and the fractional quantum Hall effect, Phys. Rev. B **61**, 10267 (2000).

[2] A. Y. Kitaev, Unpaired Majorana fermions in quantum wires, Phys. Usp. **44**, 131 (2001).

[3] C. Nayak, S. H. Simon, A. Stern, M. Freedman, and S. Das Sarma, Non-Abelian anyons and topological quantum computation, Rev. Mod. Phys. **80**, 1083 (2008).

[4] J. Alicea, New directions in the pursuit of Majorana fermions in solid state systems, Rep. Prog. Phys. **75**, 076501 (2012).

[5] M. Leijnse and K. Flensberg, Introduction to topological superconductivity and Majorana fermions, Semicond. Sci. Technol. **27**, 124003 (2012).

[6] C. W. J. Beenakker, Search for Majorana fermions in superconductors, Annu. Rev. Condens. Matter Phys. **4**, 113 (2013).

[7] T. D Stanescu and S. Tewari, Majorana fermions in semiconductor nanowires: Fundamentals, modeling, and experiment, J. Phys.: Condens. Matter **25**, 233201 (2013).

[8] J.-H. Jiang and S. Wu, Non-Abelian topological superconductors from topological semimetals and related systems under the superconducting proximity effect, J. Phys.: Condens. Matter **25**, 055701 (2013).

[9] S. D. Sarma, M. Freedman, and C. Nayak, Majorana zero modes and topological quantum computation, npj Quantum Inf. **1**, 15001 (2015).

[10] S. R. Elliott and M. Franz, Colloquium: Majorana fermions in nuclear, particle, and solid-state physics, Rev. Mod. Phys. **87**, 137 (2015).

[11] M. Sato and S. Fujimoto, Majorana fermions and topology in superconductors, J. Phys. Soc. Jpn. **85**, 072001 (2016).

[12] M. Sato and Y. Ando, Topological superconductors: A review, Rep. Prog. Phys. **80**, 076501 (2017).

[13] R. M. Lutchyn, E. P. A. M. Bakkers, L. P. Kouwenhoven, P. Krogstrup, C. M. Marcus, and Y. Oreg, Majorana zero modes in superconductor–semiconductor heterostructures, Nat. Rev. Mater. **3**, 52 (2018).

[14] H. Zhang, D. E. Liu, M. Wimmer, and L. P. Kouwenhoven, Next steps of quantum transport in Majorana nanowire devices, Nat. Commun. **10**, 5128 (2019).

[15] K. Flensberg, F. von Oppen, and A. Stern, Engineered platforms for topological superconductivity and Majorana zero modes, Nat. Rev. Mater. **6**, 944 (2021).

[16] S. Das Sarma, In search of Majorana, Nat. Phys. **19**, 165 (2023).

[17] J. D. Sau and S. D. Sarma, Realizing a robust practical Majorana chain in a quantum-dot-superconductor linear array, Nat. Commun. **3**, 964 (2012).

[18] H. Pan and S. Das Sarma, Physical mechanisms for zero-bias conductance peaks in Majorana nanowires, Phys. Rev. Res. **2**, 013377 (2020).

[19] S. Ahn, H. Pan, B. Woods, T. D. Stanescu, and S. Das Sarma, Estimating disorder and its adverse effects in semiconductor Majorana nanowires, Phys. Rev. Mater. **5**, 124602 (2021).

[20] S. Das Sarma, J. D. Sau, and T. D. Stanescu, Spectral properties, topological patches, and effective phase diagrams of finite disordered Majorana nanowires, Phys. Rev. B **108**, 085416 (2023).

[21] S. Das Sarma and H. Pan, Density of states, transport, and topology in disordered Majorana nanowires, Phys. Rev. B **108**, 085415 (2023).

[22] J. R. Taylor, J. D. Sau, and S. Das Sarma, Machine learning the disorder landscape of Majorana nanowires, Phys. Rev. Lett. **132**, 206602 (2024).

[23] C.-X. Liu, G. Wang, T. Dvir, and M. Wimmer, Tunable superconducting coupling of quantum dots via Andreev bound states in semiconductor-superconductor nanowires, Phys. Rev. Lett. **129**, 267701 (2022).

[24] A. Bordin, G. Wang, C.-X. Liu, S. L. D. ten Haaf, N. van Loo, G. P. Mazur, D. Xu, D. van Driel, F. Zatelli, S. Gazibegovic, G. Badawy, E. P. A. M. Bakkers, M. Wimmer, L. P. Kouwenhoven, and T. Dvir, Tunable crossed Andreev reflection and elastic cotunneling in hybrid nanowires, Phys. Rev. X **13**, 031031 (2023).

[25] G. Wang, T. Dvir, G. P. Mazur, C.-X. Liu, N. van Loo, S. L. D. ten Haaf, A. Bordin, S. Gazibegovic, G. Badawy, E. P. A. M. Bakkers, M. Wimmer, and L. P. Kouwenhoven, Singlet and triplet Cooper pair splitting in hybrid superconducting nanowires, Nature (London) **612**, 448 (2022).

[26] Q. Wang, S. L. D. ten Haaf, I. Kulesh, D. Xiao, C. Thomas, M. J. Manfra, and S. Goswami, Triplet correlations in Cooper pair splitters realized in a two-dimensional electron gas, Nat. Commun. **14**, 4876 (2023).

[27] A. Bordin, X. Li, D. van Driel, J. C. Wolff, Q. Wang, S. L. D. ten Haaf, G. Wang, N. van Loo, L. P. Kouwenhoven, and T. Dvir, Crossed Andreev reflection and elastic cotunneling in three quantum dots coupled by superconductors, Phys. Rev. Lett. **132**, 056602 (2024).

[28] M. Leijnse and K. Flensberg, Parity qubits and poor man's Majorana bound states in double quantum dots, Phys. Rev. B **86**, 134528 (2012).

[29] T. Dvir, G. Wang, N. van Loo, C.-X. Liu, G. P. Mazur, A. Bordin, S. L. D. ten Haaf, J.-Y. Wang, D. van Driel, F. Zatelli, X. Li, F. K. Malinowski, S. Gazibegovic, G. Badawy, E. P. A. M. Bakkers, M. Wimmer, and L. P. Kouwenhoven, Realization of a minimal Kitaev chain in coupled quantum dots, Nature (London) **614**, 445 (2023).

[30] F. Zatelli, D. van Driel, D. Xu, G. Wang, C.-X. Liu, A. Bordin, B. Roovers, G. P. Mazur, N. van Loo, J. C. Wolff *et al.*, Robust poor man's Majorana zero modes using Yu-Shiba-Rusinov states, Nat. Commun. **15**, 7933 (2024).

[31] A. Bordin, C.-X. Liu, T. Dvir, F. Zatelli, S. L. ten Haaf, D. van Driel, G. Wang, N. van Loo, T. van Caekenberghe, J. C. Wolff *et al.*, Signatures of Majorana protection in a three-site Kitaev chain, arXiv:2402.19382.

[32] S. L. D. ten Haaf, Q. Wang, A. M. Bozkurt, C.-X. Liu, I. Kulesh, P. Kim, D. Xiao, C. Thomas, M. J. Manfra, T. Dvir, M. Wimmer, and S. Goswami, A two-site Kitaev chain in a two-dimensional electron gas, Nature (London) **630**, 329 (2024).

[33] J. D. Sau and S. D. Sarma, Capacitance-based fermion parity read-out and predicted Rabi oscillations in a Majorana nanowire, arXiv:2406.18080.

[34] C.-X. Liu, H. Pan, F. Setiawan, M. Wimmer, and J. D. Sau, Fusion protocol for Majorana modes in coupled quantum dots, Phys. Rev. B **108**, 085437 (2023).

[35] P. Boross and A. Pályi, Braiding-based quantum control of a Majorana qubit built from quantum dots, Phys. Rev. B **109**, 125410 (2024).

[36] A. Tsintzis, R. S. Souto, K. Flensberg, J. Danon, and M. Leijnse, Majorana qubits and non-Abelian physics in quantum dot–based minimal Kitaev chains, PRX Quantum **5**, 010323 (2024).

[37] V. Mourik, K. Zuo, S. M. Frolov, S. R. Plissard, E. P. A. M. Bakkers, and L. P. Kouwenhoven, Signatures of Majorana fermions in hybrid superconductor-semiconductor nanowire devices, Science **336**, 1003 (2012).

[38] F. Nichele, A. C. C. Drachmann, A. M. Whiticar, E. C. T. O'Farrell, H. J. Suominen, A. Fornieri, T. Wang, G. C. Gardner, C. Thomas, A. T. Hatke, P. Krogstrup, M. J. Manfra, K. Flensberg, and C. M. Marcus, Scaling of Majorana zero-bias conductance peaks, Phys. Rev. Lett. **119**, 136803 (2017).

[39] H. Zhang, M. W. A. de Moor, J. D. S. Bommer, D. Xu, G. Wang, N. van Loo, C.-X. Liu, S. Gazibegovic, J. A. Logan, D. Car *et al.*, Large zero-bias peaks in InSb-Al hybrid semiconductor-superconductor nanowire devices, arXiv:2101.11456.

[40] M. Aghaee, A. Akkala, Z. Alam, R. Ali, A. Alcaraz Ramirez, M. Andrzejczuk, A. E. Antipov, P. Aseev, M. Astafev, B. Bauer, J. Becker, S. Boddapati, F. Boekhout, J. Bommer, T. Bosma, L. Bourdet, S. Boutin, P. Caroff, L. Casparis, M. Cassidy, S. Chatoor, A. W. Christensen, N. Clay, W. S. Cole, F. Corsetti, A. Cui, P. Dalampiras, A. Dokania, G. de Lange, M. de Moor, J. C. Estrada Saldaña, S. Fallahi, Z. H. Fathabad, J. Gamble, G. Gardner, D. Govender, F. Griggio, R. Grigoryan, S. Gronin, J. Gukelberger, E. B. Hansen, S. Heedt, J. Herranz Zamorano, S. Ho, U. L. Holgaard, H. Ingerslev, L. Johansson, J. Jones, R. Kallaher, F. Karimi, T. Karzig, E. King, M. E. Kloster, C. Knapp, D. Kocon, J. Koski, P. Kostamo, P. Krogstrup, M. Kumar, T. Laeven, T. Larsen, K. Li, T. Lindemann, J. Love, R. Lutchyn, M. H. Madsen, M. Manfra, S. Markussen, E. Martinez, R. McNeil, E. Memisevic, T. Morgan, A. Mullally, C. Nayak, J. Nielsen, W. H. P. Nielsen, B. Nijholt, A. Nurmohamed, E. O'Farrell, K. Otani, S. Pauka, K. Petersson, L. Petit, D. I. Pikulin, F. Preiss, M. Quintero-Perez, M. Rajpalke, K. Rasmussen, D. Razmadze, O. Reentila, D. Reilly, R. Rouse, I. Sadovskyy, L. Sainiemi, S. Schreppler, V. Sidorkin, A. Singh, S. Singh, S. Sinha, P. Sohr, T. Stankevič, L. Stek, H. Suominen, J. Suter, V. Svidenko, S. Teicher, M. Temuerhan, N. Thiyagarajah, R. Tholapi, M. Thomas, E. Toomey, S. Upadhyay, I. Urban, S. Vaitiekėnas, K. Van Hoogdalem, D. Van Woerkom, D. V. Viazmitinov, D. Vogel, S. Waddy, J. Watson, J. Weston, G. W. Winkler, C. K. Yang, S. Yau, D. Yi, E. Yucelen, A. Webster, R. Zeisel, and R. Zhao(Microsoft Quantum), InAs-Al hybrid devices passing the topological gap protocol, Phys. Rev. B **107**, 245423 (2023).

[41] J. D. Sau, R. M. Lutchyn, S. Tewari, and S. Das Sarma, Generic new platform for topological quantum computation using semiconductor heterostructures, Phys. Rev. Lett. **104**, 040502 (2010).

[42] R. M. Lutchyn, J. D. Sau, and S. Das Sarma, Majorana fermions and a topological phase transition in semiconductor-superconductor heterostructures, Phys. Rev. Lett. **105**, 077001 (2010).

[43] Y. Oreg, G. Refael, and F. von Oppen, Helical liquids and Majorana bound states in quantum wires, Phys. Rev. Lett. **105**, 177002 (2010).

[44] X. Hu and S. Das Sarma, Charge-fluctuation-induced dephasing of exchange-coupled spin qubits, Phys. Rev. Lett. **96**, 100501 (2006).

[45] K. D. Petersson, J. R. Petta, H. Lu, and A. C. Gossard, Quantum coherence in a one-electron semiconductor charge qubit, Phys. Rev. Lett. **105**, 246804 (2010).

[46] O. E. Dial, M. D. Shulman, S. P. Harvey, H. Bluhm, V. Umansky, and A. Yacoby, Charge noise spectroscopy using coherent exchange oscillations in a singlet-triplet qubit, Phys. Rev. Lett. **110**, 146804 (2013).

[47] P. Scarlino, J. H. Ungerer, D. J. van Woerkom, M. Mancini, P. Stano, C. Müller, A. J. Landig, J. V. Koski, C. Reichl, W. Wegscheider, T. Ihn, K. Ensslin, and A. Wallraff, *In situ* tuning of the electric-dipole strength of a double-dot charge qubit: Charge-noise protection and ultrastrong coupling, Phys. Rev. X **12**, 031004 (2022).

[48] E. J. Connors, J. Nelson, L. F. Edge, and J. M. Nichol, Charge-noise spectroscopy of Si/SiGe quantum dots via dynamically-decoupled exchange oscillations, Nat. Commun. **13**, 940 (2022).

[49] R. E. Throckmorton and S. Das Sarma, Crosstalk- and charge-noise-induced multiqubit decoherence in exchange-coupled quantum dot spin qubit arrays, Phys. Rev. B **105**, 245413 (2022).

[50] G. Burkard, T. D. Ladd, A. Pan, J. M. Nichol, and J. R. Petta, Semiconductor spin qubits, Rev. Mod. Phys. **95**, 025003 (2023).

[51] E. Paladino, Y. M. Galperin, G. Falci, and B. L. Altshuler, $1/f$ noise: Implications for solid-state quantum information, Rev. Mod. Phys. **86**, 361 (2014).

[52] G. Ithier, E. Collin, P. Joyez, P. J. Meeson, D. Vion, D. Esteve, F. Chiarello, A. Shnirman, Y. Makhlin, J. Schriefl, and G. Schön, Decoherence in a superconducting quantum bit circuit, Phys. Rev. B **72**, 134519 (2005).

[53] P. Boross and A. Pályi, Dephasing of Majorana qubits due to quasistatic disorder, Phys. Rev. B **105**, 035413 (2022).

[54] T. Hayashi, T. Fujisawa, H. D. Cheong, Y. H. Jeong, and Y. Hirayama, Coherent manipulation of electronic states in a double quantum dot, Phys. Rev. Lett. **91**, 226804 (2003).

[55] C.-X. Liu, A. M. Bozkurt, F. Zatelli, S. L. D. ten Haaf, T. Dvir, and M. Wimmer, Enhancing the excitation gap of a quantum-dot-based Kitaev chain, Commun. Phys. **7**, 235 (2024).

[56] Y. Luh, Bound state in superconductors with paramagnetic impurities, Acta Phys. Sin. **21**, 75 (1965).

[57] H. Shiba, Classical spins in superconductors, Prog. Theor. Phys. **40**, 435 (1968).

[58] A. Rusinov, Theory of gapless superconductivity in alloys containing paramagnetic impurities, Sov. Phys. JETP **29**, 1101 (1969).

[59] M. Aghaee, A. A. Ramirez, Z. Alam, R. Ali, M. Andrzejczuk, A. Antipov, M. Astafev, A. Barzegar, B. Bauer, J. Becker *et al.*, Interferometric single-shot parity measurement in an inas-al hybrid device, arXiv:2401.09549.

[60] C.-X. Liu, S. Miles, A. Bordin, S. L. D. ten Haaf, A. M. Bozkurt, and M. Wimmer, Protocol for scaling up a sign-ordered Kitaev chain without magnetic flux control, arXiv:2407.04630.